Available online at www.sciencedirect.com

ScienceDirect

Geochimica et Cosmochimica Acta 259 (2019) 413

Geochimica et Cosmochimica Acta

www.elsevier.com/locate/gca

Corrigendum

Corrigendum to "Multicomponent diffusion in basaltic melts at 1350 °C" [Geochim. Cosmochim. Acta 228 (2018) 190–204]

The authors regret that the errors on the [D] matrix in Table 7 should be corrected as follows:
Table 7 (using 10 experiments)

D ($\mu m^2/s$)	TiO_2	Al_2O_3	MgO	CaO	Na_2O	K_2O
TiO_2	18.78 ± 0.32	−0.81 ± 0.23	−4.20 ± 0.47	−11.10 ± 1.16	−27.13 ± 2.85	−15.54 ± 3.27
Al_2O_3	−4.72 ± 0.96	8.96 ± 0.43	−17.40 ± 0.96	−36.01 ± 1.95	−60.32 ± 4.74	−80.65 ± 5.33
MgO	−6.77 ± 1.13	0.22 ± 0.58	39.02 ± 1.23	−39.62 ± 2.38	−82.61 ± 5.54	−45.38 ± 7.01
CaO	−11.20 ± 1.30	−4.56 ± 0.62	−27.62 ± 1.29	64.89 ± 2.58	−31.03 ± 5.49	30.37 ± 7.40
Na_2O	27.40 ± 1.25	11.66 ± 0.64	48.66 ± 1.28	59.90 ± 1.83	341.56 ± 3.92	98.05 ± 6.13
K_2O	5.39 ± 0.50	5.98 ± 0.22	11.67 ± 0.46	15.20 ± 0.93	−0.37 ± 1.88	114.29 ± 2.43

These corrections do not affect other parts of the paper. The authors would like to apologize for any inconvenience caused.

Chenghuan Guo (郭城桓) Department of Earth and Environmental Sciences, The University of Michigan, Ann Arbor, MI 48109-1005, USA

Youxue Zhang (张有学) Department of Earth and Environmental Sciences, The University of Michigan, Ann Arbor, MI 48109-1005, USA

DOI of original article: 10.1016/j.gca.2018.02.043.

https://doi.org/10.1016/j.gca.2019.06.010
0016-7037/© 2018 Elsevier Ltd. All rights reserved.

Available online at www.sciencedirect.com

ScienceDirect

Geochimica et Cosmochimica Acta 228 (2018) 190–204

Geochimica et Cosmochimica Acta

www.elsevier.com/locate/gca

Multicomponent diffusion in basaltic melts at 1350 °C

Chenghuan Guo (郭城桓) *, Youxue Zhang (张有学)

Department of Earth and Environmental Sciences, The University of Michigan, Ann Arbor, MI 48109-1005, USA

Received 13 April 2017; accepted in revised form 25 February 2018; Available online 6 March 2018

Abstract

Nine successful diffusion couple experiments were conducted in an 8-component SiO_2–TiO_2–Al_2O_3–FeO–MgO–CaO–Na_2O–K_2O system at ~1350 °C and at 1 GPa, to study multicomponent diffusion in basaltic melts. At least 3 traverses were measured to obtain diffusion profiles for each experiment. Multicomponent diffusion matrix at 1350 °C was obtained by simultaneously fitting diffusion profiles of diffusion couple experiments. Furthermore, in order to better constrain the diffusion matrix and reconcile mineral dissolution data, mineral dissolution experiments in the literature and diffusion couple experiments from this study, were fit together. All features of diffusion profiles in both diffusion couple and mineral dissolution experiments were well reproduced by the diffusion matrix. Diffusion mechanism is inferred from eigenvectors of the diffusion matrix, and it shows that the diffusive exchange between network-formers SiO_2 and Al_2O_3 is the slowest, the exchange of SiO_2 with other oxide components is the second slowest with an eigenvalue that is only ~10% larger, then the exchange between divalent oxide components and all the other oxide components is the third slowest with an eigenvalue that is twice the smallest eigenvalue, then the exchange of FeO + K_2O with all the other oxide components is the fourth slowest with an eigenvalue that is 5 times the smallest eigenvalue, then the exchange of MgO with FeO + CaO is the third fastest with an eigenvalue that is 6.3 times the smallest eigenvalue, then the exchange of CaO + K_2O with all the other oxide components is the second fastest with an eigenvalue that is 7.5 times the smallest eigenvalue, and the exchange of Na_2O with all other oxide components is the fastest with an eigenvalue that is 31 times the smallest eigenvalue. The slowest and fastest eigenvectors are consistent with those for simpler systems in most literature. The obtained diffusion matrix was successfully applied to predict diffusion profiles during mineral dissolution in basaltic melts.
© 2018 Elsevier Ltd. All rights reserved.

Keywords: Diffusion kinetics; Natural basalt; Diffusion eigenvectors; Diffusion eigenvalues; 8-component systems

1. INTRODUCTION

Numerous major components are present in natural silicate melts (e.g. SiO_2, TiO_2, Al_2O_3, FeO, MgO, CaO, Na_2O and K_2O). Therefore, multicomponent diffusion is of fundamental significance in natural processes involving mass transport, such as magma mixing and contamination (Sato, 1975; Watson, 1982; Koyaguchi, 1985, 1989; Oldenburg et al., 1989), magma double-diffusive convection (Turner, 1985; Liang et al., 1994; Richter et al., 1998), and mineral growth or dissolution in magmas (Watson, 1982; Zhang et al., 1989).

Effective binary diffusion treatment (Cooper, 1968) has been widely used as an alternative to treat monotonic concentration profiles for diffusion in a multicomponent system. However, it cannot handle the often-observed uphill diffusion profiles in natural melts (Sato, 1975; Watson, 1982; Zhang et al., 1989), although some empirical models have been proposed for quantifying uphill diffusion (Cooper, 1968; Lasaga, 1979; Richter, 1993; Zhang, 1993; Liang et al., 1997). In addition, effective binary diffusion coefficient of a given component depends strongly on concentration gradients of other components (Cooper, 1968;

* Corresponding author.
E-mail address: chguo@umich.edu (C. Guo).

https://doi.org/10.1016/j.gca.2018.02.043
0016-7037/© 2018 Elsevier Ltd. All rights reserved.

Zhang et al., 1989; Liang et al., 1996; Chen and Zhang, 2008, 2009; Guo and Zhang, 2016), making it difficult to use the approach. Therefore, multicomponent diffusion treatment is required for a more accurate quantification of diffusion in natural melts.

Tremendous efforts have been made in studying multicomponent diffusion in both synthetic and natural silicate melt systems: SiO_2–Al_2O_3–CaO, SiO_2–Al_2O_3–MgO, SiO_2–Al_2O_3–K_2O, SiO_2–CaO–Na_2O, SiO_2–B_2O_3–Na_2O, SiO_2–Al_2O_3–MgO–CaO, SiO_2–Al_2O_3–Na_2O–K_2O, SiO_2–Al_2O_3–Na_2O–K_2O–H_2O, SiO_2–TiO_2–Al_2O_3–FeO–MgO–CaO, and SiO_2–TiO_2–Al_2O_3–MgO–CaO–Na_2O–K_2O (Sugawara et al., 1977; Oishi et al., 1982; Kress and Ghiorso, 1993, 1995; Chakraborty et al., 1995; Liang et al. 1996; Mungall et al., 1998; Richter et al., 1998; Liang and Davis, 2002; Liang, 2010; Watkins et al., 2014; Claireaux et al., 2016; Guo and Zhang, 2016; Pablo et al., 2017). Diffusion matrices in simple silicate melt systems or partial diffusion matrices in natural silicate melt systems have been obtained (e.g., Kress and Ghiorso, 1995; Mungall et al., 1998; Morgan et al., 2006; Guo and Zhang, 2016). However, they have not been successfully applied to predict diffusion in natural melts, such as during mineral dissolution (e.g. Fig. 1 in Guo and Zhang, 2016). Several empirical models have been proposed to calculate multicomponent diffusion matrix (Lasaga, 1979; Richter 1993; Liang et al, 1997), by which diffusion profiles during mineral dissolution are calculated (Alexander, 2011). However, only limited success is achieved in predicting diffusion in natural melts by those empirical models (e.g. Fig. 2 in Guo and Zhang, 2016).

To better understand major-component diffusion in natural silicate melts, or more specifically basaltic melts, and as a follow-up study of our previous work on a haplobasaltic melt (Guo and Zhang, 2016), we investigated multicomponent diffusion by diffusion couple experiments in an 8-component SiO_2–TiO_2–Al_2O_3–FeO–MgO–CaO–Na_2O–K_2O system at 1350 °C and at 1 GPa. Experiments were carried out and combined with literature data to determine the 7 × 7 diffusion matrix. From the diffusion matrix, diffusion eigenvectors are used to discuss diffusion mechanisms, and diffusion profiles during mineral dissolution are predicted.

2. EXPERIMENTAL STRATEGY AND ANALYTICAL METHODS

2.1. Diffusion couple experiments

The 8-component SiO_2–TiO_2–Al_2O_3–FeO–MgO–CaO–Na_2O–K_2O basaltic melts have an average composition of 51% SiO_2, 2% TiO_2, 14% Al_2O_3, 11.5% FeO, 6.5% MgO, 10.5% CaO, 3% Na_2O, 1.5% K_2O (in wt%), shown as "Base Comp" in Table 1. This composition will be referred to as "base" hereafter. The base was chosen to be close to the composition of Juan de Fuca (JDF) mid-ocean ridge basalts (MORB): 50.98% SiO_2, 1.97% TiO_2, 13.81% Al_2O_3, 12.24% FeO, 7.15% MgO, 10.91% CaO, 2.77% Na_2O, 0.17% K_2O

Table 1
Average compositions (in wt%), 1σ errors and liquidus of initial glasses.

	SiO_2^* ave(σ)	TiO_2 ave(σ)	Al_2O_3 ave(σ)	FeO_t ave(σ)	MgO ave(σ)	CaO ave(σ)	Na_2O ave(σ)	K_2O ave(σ)	Total	Liquidus °C
Base comp	51.00	2.00	14.00	11.50	6.50	10.50	3.00	1.50	100	1317
JDF basalts	50.98	1.97	13.81	12.24	7.15	10.91	2.77	0.17	100	1331
Haplobasalts	50.00	1.50	15.00	0.00	10	19.00	3.00	1.50	100	1367
BS1	51.74(23)	0.51(2)	14.17(10)	11.60(10)	6.70(5)	10.78(29)	3.03(6)	1.48(3)	100	1324
BS2	49.46(16)	3.37(6)	14.18(12)	11.20(10)	6.64(6)	10.68(09)	3.01(5)	1.45(2)	100	1309
BS3	51.79(15)	1.95(3)	12.76(05)	11.72(08)	6.64(5)	10.69(12)	2.99(4)	1.46(3)	100	1325
BS4	49.16(14)	1.96(5)	15.73(07)	11.46(07)	6.70(5)	10.56(10)	2.99(3)	1.44(3)	100	1307
BS5	52.16(17)	1.97(5)	14.19(06)	9.90(16)	6.57(7)	10.57(10)	3.10(5)	1.54(4)	100	1322
BS6	49.16(23)	1.96(6)	14.32(06)	12.84(08)	6.68(7)	10.54(06)	3.03(3)	1.51(4)	100	1311
BS7	51.97(15)	1.94(4)	14.30(09)	11.44(07)	5.33(4)	10.62(06)	3.00(3)	1.40(1)	100	1304
BS8	49.15(24)	1.95(6)	14.29(08)	11.40(13)	8.13(8)	10.55(09)	3.01(4)	1.52(3)	100	1330
BS9	51.69(10)	1.95(7)	14.39(09)	11.33(11)	6.60(6)	9.21(08)	3.21(5)	1.61(3)	100	1330
BS10	49.19(16)	2.00(5)	14.17(05)	11.36(08)	6.67(8)	11.99(09)	3.07(3)	1.56(3)	100	1321
BS11	52.19(18)	2.01(5)	14.07(06)	11.30(10)	6.77(4)	10.56(08)	1.55(2)	1.55(2)	100	1339
BS12	49.31(18)	2.00(3)	14.07(09)	11.38(13)	6.70(3)	10.53(07)	4.48(5)	1.53(3)	100	1315
BS13	52.54(23)	1.97(6)	13.94(12)	11.31(07)	6.67(8)	10.52(08)	3.01(6)	0.05(1)	100	1320
BS14	49.18(13)	2.01(5)	13.94(08)	11.62(07)	6.60(5)	10.53(09)	3.06(3)	3.06(7)	100	1317
BS17	51.21(24)	1.97(4)	13.95(17)	11.17(14)	8.00(9)	10.62(05)	3.05(4)	0.04(1)	100	1354
BS18	51.02(19)	1.96(4)	13.83(10)	11.46(14)	5.24(4)	10.52(06)	2.99(4)	2.98(3)	100	1309
BS19	51.11(27)	2.00(5)	15.39(21)	11.33(13)	6.59(7)	9.05(07)	3.04(4)	1.48(2)	100	1328
BS20	51.29(21)	1.98(5)	12.42(14)	11.38(14)	6.61(5)	11.84(07)	2.98(5)	1.50(3)	100	1331

Note:
1. SiO_2^* is define as $SiO_2^* = SiO_2 - (\text{total} - 100)$, so that the new "total" is 100%.
2. The values in parentheses are 1σ errors on the last digit.
3. Liquidus of initial glasses at 1 GPa were estimated by the MELTS program (Ghiorso and Sack, 1995; Asimow and Ghiorso, 1998).
4. The composition of 7–component haplobasaltic melts for which diffusion matrix at 1500 °C and 1 GPa was determined by Guo and Zhang (2016) is also listed for comparison and discussion.

(in wt%), shown as "JDF Basalts" in Table 1 (Dixon et al., 1986, 1988), except for a significantly higher K_2O concentration for our experimental composition so as to better resolve the role of K_2O in multicomponent diffusion. A MORB composition was chosen because mid-ocean ridge magmatism is the most abundant magmatic activity on Earth. Diffusion couples were designed in such a way that: for each diffusion couple, one half deviates from the base by +1.5 wt% in one oxide component and –1.5 wt% in another oxide component, and the other half deviates by –1.5 wt% and +1.5 wt% in the same two oxide components for complementariness. Therefore, the compositional variation between the two halves is present in only two components. The 3.0-wt% compositional variation for two oxide components in one couple was chosen to optimize the tradeoff between measurable diffusion profiles and negligible compositional dependence of the diffusion matrix.

The initial glasses for each half of diffusion couple were synthesized in a Deltech furnace at the University of Michigan. SiO_2, TiO_2, Al_2O_3, FeO, MgO, CaO, Na_2CO_3 and K_2CO_3 powders were weighed in the designed proportions, grinded in a mortar, mixed in ethanol and dried in a desiccator in vacuum. Mixed powders were placed in a glassy carbon crucible, heated up to 1450 °C at a programmed rate under N_2 flow at 1 atm, kept there at 1450 °C for 2 hours to homogenize and then quenched in air. The average compositions of initial glasses are shown in Table 1. The ferric/ferrous iron ratio is measured by XANES, and $4 \pm 1\%$ iron is ferric iron. Two complimentary compositions, such as BS1 and BS2, are put together to make a diffusion couple BS1&2.

Synthesized glasses were cut and shaped into cylinders with diameter of ~2 mm. Cylinders were sliced into disks with thickness of 1.5–2.0 mm (depending on estimated diffusion distance of the fastest diffusion component). Sample disks were polished on one side. Two sample disks were placed into a graphite capsule. Densities of initial glasses at 1350 °C and 1 GPa were estimated by Lange and Carmichael (1990), and the less dense sample disk in each diffusion couple was placed on top of the denser one to suppress convection. The graphite capsule was placed into an MgO rod. The MgO rod was placed into a graphite heater. The graphite heater was placed into a $BaCO_3$ pressure medium. This is called a sample assembly. The same design was used for all experiments to maintain consistency of actual temperatures among different experiments.

Chemical diffusion couple experiments were conducted in a ½-inch piston-cylinder apparatus at the University of Michigan, at ~1350 °C and at 1 GPa. The temperature was chosen to be higher than the estimated liquidus of all initial glasses (Table 1) by the MELTS program (Ghiorso and Sack, 1995; Asimow and Ghiorso, 1998). Temperature was controlled by a type-S thermocouple. The tip of the thermocouple was covered by alumina cement and separated from the graphite capsule by an MgO wafer with thickness of ~0.5 mm. The target controller (thermocouple) temperature was estimated so as to reach 1350 °C at the center (interface) of the diffusion couple based on the temperature calibration of Hui et al. (2008).

Experimental procedures are as follows. First, the sample assembly is brought to a pressure 10–15% higher than the target pressure, and then relaxed at 200 °C overnight (>12 h). After relaxation, the pressure is decreased to the target pressure (piston-out procedure). Then, temperature is increased at a programmed rate to the target temperature within 1 minute. The sample assembly is kept at the target temperature and pressure for a planned duration, until quenched by turning off the power.

Both temperature and pressure were continuously recorded. Temperature fluctuation was less than 1 °C and pressure was manually controlled with a fluctuation of ~10 MPa. Actual temperature was calculated based on the post-experiment distance between the thermocouple tip and the center of diffusion couple using the calibration by Hui et al. (2008), which is typically slightly different from planned temperature due to a variable distance between the center of the diffusion couple and the thermocouple tip. Pressure was corrected by dividing the nominal pressure by 1.06 (Hui et al., 2008; Ni and Zhang, 2008). Experimental conditions are listed in Table 2.

After experiments, the sample assembly was embedded in epoxy, grounded, polished and carbon coated. Diffusion profiles were measured at 15 kV using a 10nA beam by a Cameca SX100 electron microprobe at Electron Microbeam Analysis Laboratory of the University of Michigan, where mass fraction (wt%) instead of mole fraction was used as concentration. Analytical conditions are listed in Table S1 in supplementary file.

2.2. Mineral dissolution experiments

During mineral dissolution in a natural melt, multicomponent diffusion profiles are also generated. These diffusion profiles are critical for understanding mineral dissolution kinetics, but also provide constraints on multicomponent diffusion matrix, and offer data for testing diffusion matrix obtained for a given bulk melt composition. On the other hand, in mineral dissolution experiments, the interface melt composition is dictated by mineral-melt equilibrium, meaning both the total concentration variation for specific components and the direction of concentration gradients cannot be precisely controlled as in diffusion couple experiments. Hence, these experiments may have larger total variations in concentrations of some components, and do not satisfy the ±1.5 wt% total concentration variation as designed in diffusion couple experiments. The larger concentration variation may lead to non-negligible dependence of the diffusion matrix elements on concentrations. Nonetheless, if such data are available, they are useful in testing and constraining the diffusion matrix as long as possible complexities are recognized.

In this study, no new mineral dissolution experiments were carried out. Nonetheless, the choice of our melt composition is close to that of Juan de Fuca mid-ocean ridge basalts that was used in mineral dissolution studies of Chen and Zhang (2008, 2009) and Yu et al. (2016). Hence, we will use the literature data at similar temperatures to test and constrain the diffusion matrix.

Table 2
Summary of experimental conditions and effective binary diffusion coefficients.

Exp#	Temp °C	Duration sec	Couples	D(SiO_2) $\mu m^2/s$	D(TiO_2) $\mu m^2/s$	D(Al_2O_3) $\mu m^2/s$	D(FeO_t) $\mu m^2/s$	D(MgO) $\mu m^2/s$	D(CaO) $\mu m^2/s$	D(Na_2O) $\mu m^2/s$	D(K_2O) $\mu m^2/s$
BS1&2A	1380.9	1204.2	Si–Ti	5.1 ± 0.9	8.6 ± 0.2						
BS3&4A	1354.6	1203.5	Si–Al	4.8 ± 0.6		4.8 ± 0.3					
BS5&6A	1349.2	904.1	Si–Fe	10.6 ± 1.3			23.7 ± 1.7				
BS7&8A	1352.3	958.7	Si–Mg	13.1 ± 1.7				28.5 ± 1.2			
BS9&10A	1354.6	545.9	Si–Ca	10.1 ± 1.6					35.7 ± 1.9		
BS11&12A	1349.2	395.8	Si–Na	–						249.7 ± 7.6	
BS13&14A	1351.9	515.0	Si–K	25.6 ± 3.1							42.0 ± 1.2
BS17&18A	1349.9	336.0	Mg–K					19.8 ± 1.2			28.4 ± 1.7
BS19&20A	1354.6	335.3	Al–Ca			6.0 ± 0.9			29.3 ± 1.2		

Note:
1. All experiments were at 1.0 GPa.
2. Reported temperatures are actual experimental temperatures at the center of diffusion couples.
3. Durations are calculated effective experimental durations.
4. For easy comparison, the effective binary diffusion coefficients are not those at the experimental temperatures, but those at 1350 °C, by correcting effective experimental durations using $t_{corr} = t_{exp} \cdot e^{-E/(RT_{exp})}/e^{-E/(RT_{corr})}$ (Zhang and Behrens, 2000) where $T_{corr} = 1350$ °C and $E = 145$ kJ/mol (from unpublished data in this study).
5. D(SiO_2) for experiment BS11&12A is not listed, because this extracted value is not accurate due to asymmetric SiO_2 profile.

3. EXPERIMENTAL RESULTS

Nine successful diffusion couple experiments were carried out. The name of each diffusion couple experiment ID indicates two halves of initial glasses in the diffusion couple. For example, BS13&14A means that one half is BS13 and the other half is BS14, where "BS" stands for "basalts", and the last letter "A" indicates the experiment is at ~1350 °C. Table 3 shows the interface composition of each diffusion couple. The average of the interface compositions of the 9 diffusion couple experiments is very close to the compositions of the base and the JDF basalts. The 1σ standard deviation of the interface compositions is less than 0.55 wt% for all components.

Fig. 1 shows an optical microscopic image of sample charge BS13&14A, with 3 traverses indicated by solid lines. Two halves of initial glasses are molten together, and no crack is observed. The interface between two halves is not visible, but the physical interface could be seen near the graphite crucible as a dent or slight misalignment.

In general, quench crystals are not observed, and cracks are present in 5 out of 9 experiments. At least 3 traverses were measured to obtain diffusion profiles for each diffusion couple experiment. Fig. 2 shows diffusion profiles of BS13&14A. If cracks are present (not for Fig. 2), profiles across cracks are re-connected smoothly by comparing different traverses. All diffusion profiles, as well as microprobe analytical data points, can be found in the supplementary file. Effective experimental durations were calculated by $t_{eff} = \int e^{-E/(RT)} dt / e^{-E/(RT_{exp})}$ where the integration includes the heating-up and cooling-down segments (Zhang and Behrens, 2000) and $E = 145$ kJ/mol (from unpublished data in this study).

For well-resolved monotonic diffusion profiles, effective binary diffusion coefficients (EBDC) were obtained by fitting the data by an error function and reported in Table 2. The first 7 experiments have initial concentration differences of 3 wt% in SiO_2 and another component i, where $i = TiO_2$, Al_2O_3, FeO, MgO, CaO, Na_2O and K_2O. Those 7 experiments are the minimum requirement to obtain the 7 × 7 diffusion matrix in an 8-component system (Trial and Spera, 1994), unless the analytical precision is much higher than that of a regular electron microprobe (Liang 2010). The additional 2 experiments are for further constraint.

4. PRELIMINARY DATA PROCESSING BEFORE FITTING

The actual experimental temperatures at the center of the diffusion couple as determined after the experiment and effective experimental durations are listed in Table 2. The temperature variation is from 1349.2 to 1354.6 °C, except for one experiment BS1&2A with significant higher temperature 1380.9 °C. In order to reduce the error in simultaneously fitting diffusion profiles in all experiments at different experimental temperatures, experimental temperatures were "normalized" to 1350 °C, by correcting the effective experimental durations. Experimental durations were corrected by the relation $t_{corr} = t_{exp} \cdot e^{-E/(RT_{exp})}/e^{-E/(RT_{corr})}$,

Table 3
Interface compositions (in wt%) of diffusion couples.

	SiO_2^*	TiO_2	Al_2O_3	FeO_t	MgO	CaO	Na_2O	K_2O	Total
Base Comp	51.00	2.00	14.00	11.50	6.50	10.50	3.00	1.50	100
JDF Basalt	50.98	1.97	13.81	12.24	7.15	10.91	2.77	0.17	100
BS1&2A	50.55	1.93	14.20	11.38	6.71	10.81	2.97	1.45	100
BS3&4A	50.37	1.98	14.26	11.74	6.60	10.58	3.00	1.47	100
BS5&6A	50.53	1.96	14.32	11.51	6.56	10.51	3.08	1.53	100
BS7&8A	50.44	1.93	14.27	11.52	6.77	10.60	3.03	1.44	100
BS9&10A	50.54	1.97	14.21	11.34	6.63	10.57	3.15	1.59	100
BS11&12A	50.70	2.00	14.03	11.45	6.72	10.53	3.02	1.55	100
BS13&14A	50.80	1.98	13.95	11.47	6.65	10.51	3.08	1.56	100
BS17&18A	51.73	1.97	13.57	11.20	6.53	10.42	3.06	1.52	100
BS19&20A	51.78	2.00	13.55	11.32	6.52	10.33	3.03	1.47	100
Average	50.83	1.97	14.04	11.44	6.63	10.54	3.05	1.51	100
1σ deviation	0.54	0.03	0.30	0.15	0.09	0.13	0.05	0.05	

Note: SiO_2^* is define as $SiO_2^* = SiO_2 - (\text{total} - 100)$, so that the new "total" is 100%.

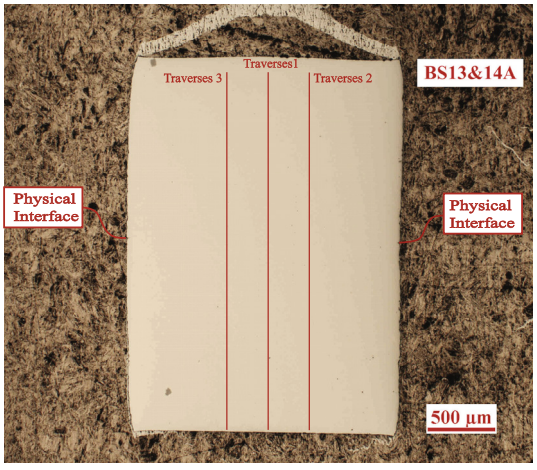

Fig. 1. Optical microscopic image of polished experimental charge BS13&14A. Three traverses (Traverse 1, Traverse 2 and Traverse 3) were measured, indicated by solid lines. Physical interface position can be seen in the image.

where $T_{corr} = 1350$ °C (Zhang and Behrens, 2000) and $E = 145$ kJ/mol (from unpublished data in this study). The corrected experimental durations were used in fitting the diffusion profiles.

We defined $SiO_2^* = SiO_2 - (\text{total} - 100)$ and used it as replacement of SiO_2 in fitting the diffusion profiles, because (1) SiO_2^* shows smaller variation than SiO_2 at the far-field, (2) SiO_2^* removes the analytical error of the "total", by attributing it to SiO_2, and (3) when using SiO_2 as the dependent component in fitting the diffusion profiles to obtain the diffusion matrix, it implicitly means SiO_2^* is used because concentrations of all components must add up to be 100%.

The boundary conditions in fitting the diffusion profiles were determined by taking average of numerous data points in the far-field. These boundary compositions can be slightly different from those average compositions of initial glasses in Table 1, due to small compositional variation in a large synthesized initial glass and small difference in day-to-day electron microprobe calibration.

The fitting is weighted nonlinear multivariable regression, and the weight is the inverse square of the analytical 1σ error of each oxide component determined by numerous data points in the far-field (which are the same data points used to determine the boundary conditions).

The interface position for each diffusion couple was determined by fitting the best diffusion profile (i.e. the diffusion profile with the largest concentration difference and the smallest 1σ error), by the following equation:

$$w = \frac{w_{-\infty} + w_{+\infty}}{2} + \frac{w_{+\infty} + w_{-\infty}}{2} \cdot \mathrm{erf}\left(\frac{x - x_0}{2\sqrt{Dt}}\right), \quad (1)$$

where w is the concentration (in wt%) of the component, $w_{-\infty}$ and $w_{+\infty}$ are the left and right side boundary conditions in the far-field, x is the position, x_0 is a rough initial estimate of the interface position, D is the effective binary diffusion coefficient, and t is the corrected experimental duration. After the interface position was determined, we defined the new position as $x_{new} = x - x_0$, such that the new interface position was at $x_{new} = 0$. The new positions were used in fitting the diffusion profiles.

5. EFFECTIVE BINARY DIFFUSION COEFFICIENTS

Effective binary diffusion coefficients (EBDC) were fit by Eq. (1) for the two components with 3-wt% concentration difference (i.e. the monotonic profiles) for each diffusion couple (Table 2). The fit is typically excellent in reproducing the data with r^2 values ranging from 0.969 to 0.999.

EBDC of a given component in a multicomponent system is strongly dependent on its counter-diffusing component in a single bulk composition, which is consistent with theoretical consideration (Cooper, 1968) and observations in Guo and Zhang (2016). Because more diffusion couples have initial concentration gradients in SiO_2, the observation is especially notable for SiO_2. EBDC of SiO_2 varies from 5.1 $\mu m^2/s$ when diffusing against TiO_2, to 25.6 $\mu m^2/s$ when diffusing against K_2O. The total variation of EBDC of SiO_2 is by a factor of 5.0. This observation indicates that application of EBDC's is of limited value and caution should be exercised when applying EBDC's,

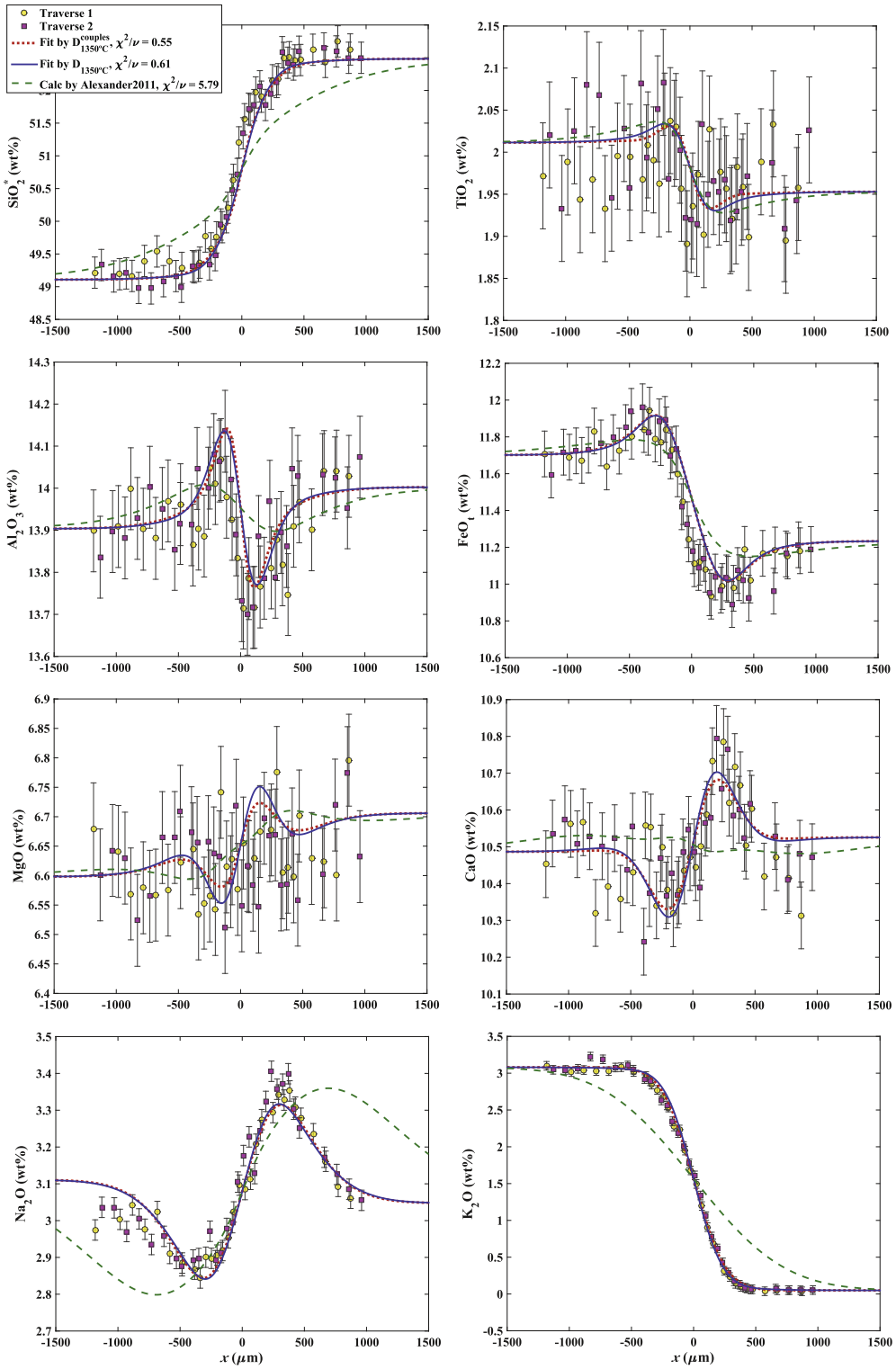

Fig. 2. Data of diffusion profiles of BS13&14A with fits. All the points are measured data. Different symbols indicate different traverses. The error bars are ±1σ errors. The long-dashed green curves are predicted profiles using the diffusion matrix given by Alexander (2011) (Note this diffusion matrix was corrected to 1350 °C for comparison). The short-dashed red curves are fit profiles for obtaining the diffusion matrix $D^{couples}_{1350°C}$ in Table 4. The solid curves are fit profiles including data from mineral dissolution experiments for obtaining the diffusion matrix $D_{1350°C}$ in Table 5. Diffusion profiles of other diffusion couple experiments with fits at ~1350 °C are shown in the supplementary file. χ^2/ν is calculated and shown for each type of fitting.

since EBDC of one component is dependent not only on the bulk melt composition, but also on its counter-diffusing component(s). To apply EBDC's to a diffusion problem, not only the bulk composition, but also the directions of the concentration gradients need to be similar. For example, EBDS's obtained from dissolution experiments of a specific mineral in a specific melt are only applicable to diffusion during the dissolution of the same mineral in the same melt.

6. FITTING DIFFUSION PROFILES OF DIFFUSION COUPLES

All diffusion profiles from 9 diffusion couple experiments were fit simultaneously using Levenberg–Marquardt–Fletc her method (LMF method) (Fletcher, 1971). The χ^2 in the following expression was minimized to obtain the diffusion matrix:

$$\chi^2 = \frac{1}{2}\sum_{k=1}^{Ne}\sum_{j=1}^{Np_k}\sum_{i=1}^{Nc}\left(\frac{w_{ijk}^{meas} - w_{ijk}^{calc}}{\sigma_{ik}}\right)^2, \quad (2)$$

where Ne is the number of experiments fit, Np_k is the number of data points in experiment k, Nc is the number of components ($Nc = 8$), w_{ijk}^{meas} and w_{ijk}^{calc} are the respectively measured and calculated concentrations of component i at position j in experiment k, and σ_{ik} is the 1σ error of w_{ijk}^{meas} (note σ_{ik} is a single number for the diffusion profile of component i in experiment k, and it is independent of position j). Each w_{ijk}^{calc} was calculated from the analytical solutions to the multicomponent diffusion equations given by eq. (A5) in Appendix A1 of Guo and Zhang (2016).

The fit diffusion matrix is denoted as $D_{1350°C}^{couples}$ and is shown in Table 4, together with eigenvalues and eigenvectors. Error of diffusion matrix was estimated by error propagation (Clifford, 1973). The short-dashed curves in Fig. 2 are the fit curves for experiment BS13&14A. All the fits by matrix $D_{1350°C}^{couples}$ for all 9 diffusion couple experiments are shown by short-dashed curves in Figs. S2–S10 in the supplementary file. It can be seen that all features in the diffusion profiles are well reproduced by this diffusion matrix. The goodness of fit for each experiment is assessed by reduced chi-square (the same as mean squares weighted deviation, MSWD).

Eigenvalues and eigenvectors of the diffusion matrices $D_{1350°C}^{couples}$ are shown in Table 4. Eigenvalues are listed in an increasing order (λ_1 always indicates the smallest eigenvalue and λ_7 always indicates the largest eigenvalue). Each column is one eigenvector in the full 8-component SiO_2–TiO_2–Al_2O_3–FeO–MgO–CaO–Na_2O–K_2O vector space (see footnote in Table 4), associated to the eigenvalue above

Table 4
Diffusion matrix $D_{1350°C}^{couples}$, obtained by fitting the 9 diffusion couple experiments at ~1350 °C, with 1σ errors for each element, and eigenvalues and eigenvectors.

$D_{1350°C}^{couples}$ ($\mu m^2/s$)	TiO_2	Al_2O_3	FeO	MgO	CaO	Na_2O	K_2O
TiO_2	8.47 ± 0.35	–0.36 ± 0.19	–2.83 ± 0.43	–1.31 ± 0.61	–1.52 ± 0.68	–4.42 ± 1.74	–1.53 ± 0.87
Al_2O_3	–1.86 ± 0.65	3.89 ± 0.32	–7.05 ± 0.60	–5.30 ± 0.99	–11.53 ± 1.19	–34.53 ± 2.80	–20.67 ± 1.45
FeO	–11.81 ± 1.46	–0.59 ± 0.74	19.98 ± 1.70	–31.48 ± 1.86	–41.17 ± 2.26	–75.38 ± 5.87	–47.71 ± 2.68
MgO	–3.60 ± 0.72	1.17 ± 0.45	–8.89 ± 0.93	24.09 ± 1.22	–18.56 ± 1.30	–34.43 ± 3.03	–6.90 ± 1.63
CaO	–2.60 ± 1.67	–2.38 ± 0.62	–9.21 ± 1.10	–7.48 ± 1.26	32.36 ± 1.44	–15.88 ± 3.97	15.98 ± 1.74
Na_2O	20.17 ± 2.03	4.07 ± 0.97	20.77 ± 1.34	40.08 ± 1.59	62.64 ± 1.67	223.75 ± 4.77	77.80 ± 1.80
K_2O	3.49 ± 0.34	1.95 ± 0.25	3.88 ± 0.55	9.10 ± 0.59	7.67 ± 0.66	7.60 ± 1.98	41.28 ± 0.91
Eigenvalues	λ_1	λ_2	λ_3	λ_4	λ_5	λ_6	λ_7
	5.07						
		6.32					
			12.22				
				33.26			
					41.01		
						49.37	
							206.58
Eigenvectors	v_1	v_2	v_3	v_4	v_5	v_6	v_7
SiO_2	–0.74	0.86	–0.40	–0.27	0.13	–0.08	–0.23
TiO_2	0.06	–0.28	–0.45	–0.07	0.03	0.04	–0.01
Al_2O_3	0.67	–0.23	–0.13	–0.17	0.02	0.04	–0.14
FeO	0.01	–0.23	0.52	0.82	–0.35	–0.61	–0.33
MgO	–0.01	–0.14	0.39	–0.24	–0.45	0.00	–0.15
CaO	0.08	–0.19	0.38	–0.30	0.80	0.72	–0.05
Na_2O	–0.02	0.09	–0.12	–0.04	–0.11	–0.26	0.89
K_2O	–0.05	0.13	–0.20	0.27	–0.08	0.16	0.02

Note: The SiO_2 component in each eigenvector is calculated from the 7–component eigenvector, by adding the SiO_2 component so that the summation of all elements in the eigenvector is zero. Then the 8–component eigenvector is renormalized. This way, the contribution by all 8 components (including the dependent component SiO_2) to each eigenvector can be directly seen.

it (e.g. v_1 is the associated eigenvector of λ_1). Eigenvalues indicate diffusivities along independent directions. Eigenvectors are often interpreted to indicate independent exchanging "species" during diffusion, i.e. the diffusion mechanism.

By examining eigenvectors of matrix $D^{couples}_{1350°C}$ (Table 4), v_1 is largely due to the exchange between SiO_2 and Al_2O_3; v_2 is largely due to the exchange between SiO_2 and all other components; v_3 is due to the exchange of FeO + MgO + CaO with all other components; v_4 is due to the exchange of FeO + K_2O with all other components; v_5 is largely due to the exchange of FeO + MgO and CaO; v_6 is largely due to the exchange of CaO + K_2O with all other components; and v_7 is due to the exchange of Na_2O (and very minor K_2O) with all other components. The relative values of eigenvalues along the eigenvectors essentially match expectations based on self or tracer diffusivities that high-valence cations and network-formers diffuse slowly, lower-valence cations and network-modifiers diffuse more rapidly, and Na and Li (low valence and small cations) have the highest diffusivity (Zhang et al., 2010).

7. PREDICTING DIFFUSION PROFILES DURING MINERAL DISSOLUTION

Predictions by matrix $D^{couples}_{1350°C}$ for major oxide diffusion profiles during olivine, diopside and anorthite dissolution (Chen and Zhang, 2008, 2009; Yu et al., 2016) using Eq. (A14) in Appendix A2 in Guo and Zhang (2016) are shown by short-dashed curves in Figs. 3–5. Theoretically, the interface melt composition in a multicomponent system can also be calculated from the diffusion matrix and the chemical potential relation between mineral and melt (Guo and Zhang, 2016). Nonetheless, in calculating diffusion profiles during mineral dissolution, the interface melt composition was determined by extrapolation of actual experimental data points in the literature, rather than by thermodynamic models such as MELTS (Ghiorso and Sack, 1995; Asimow and Ghiorso, 1998), because chemical potentials of oxides in silicate melts cannot be accurately calculated yet (e.g., Alexander, 2011). The dissolution rate was subsequently determined by solving eq. (A20) in Appendix A2 of Guo and Zhang (2016) using the extrapolated interface melt composition. Note that eq. (A20) contains $n-1$ equations, but only the equation corresponding to the best-resolved component was used to calculate the dissolution rate.

The predicted diffusion profiles (short-dashed red curves) and the experimental data match fairly well in both diffusion distances and profile shapes for SiO_2, TiO_2, Al_2O_3, FeO, MgO and CaO. The Na_2O profiles show good agreement for olivine and diopside dissolution (Figs. 3 and 4), but disagreement for anorthite dissolution (Fig. 5). The K_2O profiles are not predicted in all experiments. The disagreement is not easily explained, but might be related to the observation that K_2O is not a major component in any eigenvector (Table 4), and hence the effect of other components on K_2O diffusion is more difficult to resolve.

8. FITTING DIFFUSION PROFILES OF DIFFUSION COUPLES AND MINERAL DISSOLUTION

To better constrain the diffusion matrix and reconcile the mineral dissolution data, in addition to the 9 diffusion couple experiments, mineral dissolution experiments in basaltic melts (Exp #39, #40, #41 for olivine dissolution in Chen and Zhang, 2008; Exp #5 for diopside in Chen and Zhang, 2009; Exp #210, #212, #213, #215, #216 anorthite dissolution in Yu et al., 2016) were also used for fitting to obtain a new diffusion matrix (referred as $D_{1350°C}$ hereafter).

The mineral dissolution experiments were done at slightly different temperatures from 1350 °C. For better consistency, the experimental temperatures were "normalized" to 1350 °C, by correcting the experimental durations by relation $t_{corr} = t_{eff} \cdot e^{-E/(RT_{exp})} / e^{-E/(RT_{corr})}$ (Zhang and Behrens, 2000), where $T_{corr} = 1350$ °C and $E = 145$ kJ/mol (from unpublished data in this study). Another complexity is that the basaltic melts for mineral dissolution experiments in the literature contain minor and trace elements, which are ignored in the fitting. That is, $SiO_2^* = SiO_2 +$ minor – (total – 100) is used, such that the total is 100%.

Matrix $D_{1350°C}$ is shown in Table 5, together with eigenvalues and eigenvectors. The solid curves in Figs. 2–5 are fit curves for diffusion couple BS13&14A, olivine dissolution, diopside dissolution and anorthite dissolution. All the fits by matrix $D_{1350°C}$ for all 9 diffusion couple experiments are shown by solid curves in Figs. S2–S10 in the supplementary file. It can be seen from Figs. 2–5 and Figs. S2–S10 that all the features of diffusion profiles in diffusion couple and mineral dissolution experiments are well reproduced by matrix $D_{1350°C}$. The goodness of fit is assessed by reduced chi-squares, which shows the quality of the fits by matrix $D_{1350°C}$ for diffusion couples is slightly compromised, but still fairly close to the fits by matrix $D^{couples}_{1350°C}$.

The observation that mineral dissolution experiments with larger concentration variations across profiles (e.g., SiO_2 from 47 to 52 wt% in Fig. 5, Al_2O_3 from 14 to 24 wt % in Fig. 5, and MgO from 7 to 13 wt% in Fig. 3) can be fit well by a constant diffusion matrix means that our choice of total concentration variation of ±1.5 wt% to ensure constancy of the diffusion matrix is somewhat conservative. In the future, total concentration variation of ±2.5 wt% may be used so as to better resolve the cross diffusion terms.

Whether matrices $D^{couples}_{1350°C}$ and $D_{1350°C}$ are different can be tested by calculating $T^{couples}_{ij} = \frac{D^{couples}_{ij} - \mu_{ij}}{\sigma^{couples}_{ij}}$ and $T_{ij} = \frac{D_{ij} - \mu_{ij}}{\sigma_{ij}}$, where μ_{ij} is the weighted average of $D^{couples}_{ij}$ and D_{ij}. If matrices $D^{couples}_{1350°C}$ and $D_{1350°C}$ are statistically the same, then the shape of the histogram of $T^{couples}_{ij}$ and T_{ij} should match standard normal distribution. However, it can be seen from Fig. S1, that the shape of the histogram is different from a standard normal distribution, especially with a significant number of data outside ±2σ, which means matrices $D^{couples}_{1350°C}$ and $D_{1350°C}$ are significantly different. Diffusion matrix $D_{1350°C}$ is preferred because it is constrained by more data, and can fit and predict diffusion profiles in diffusion-couple experiments and mineral dissolution experiments.

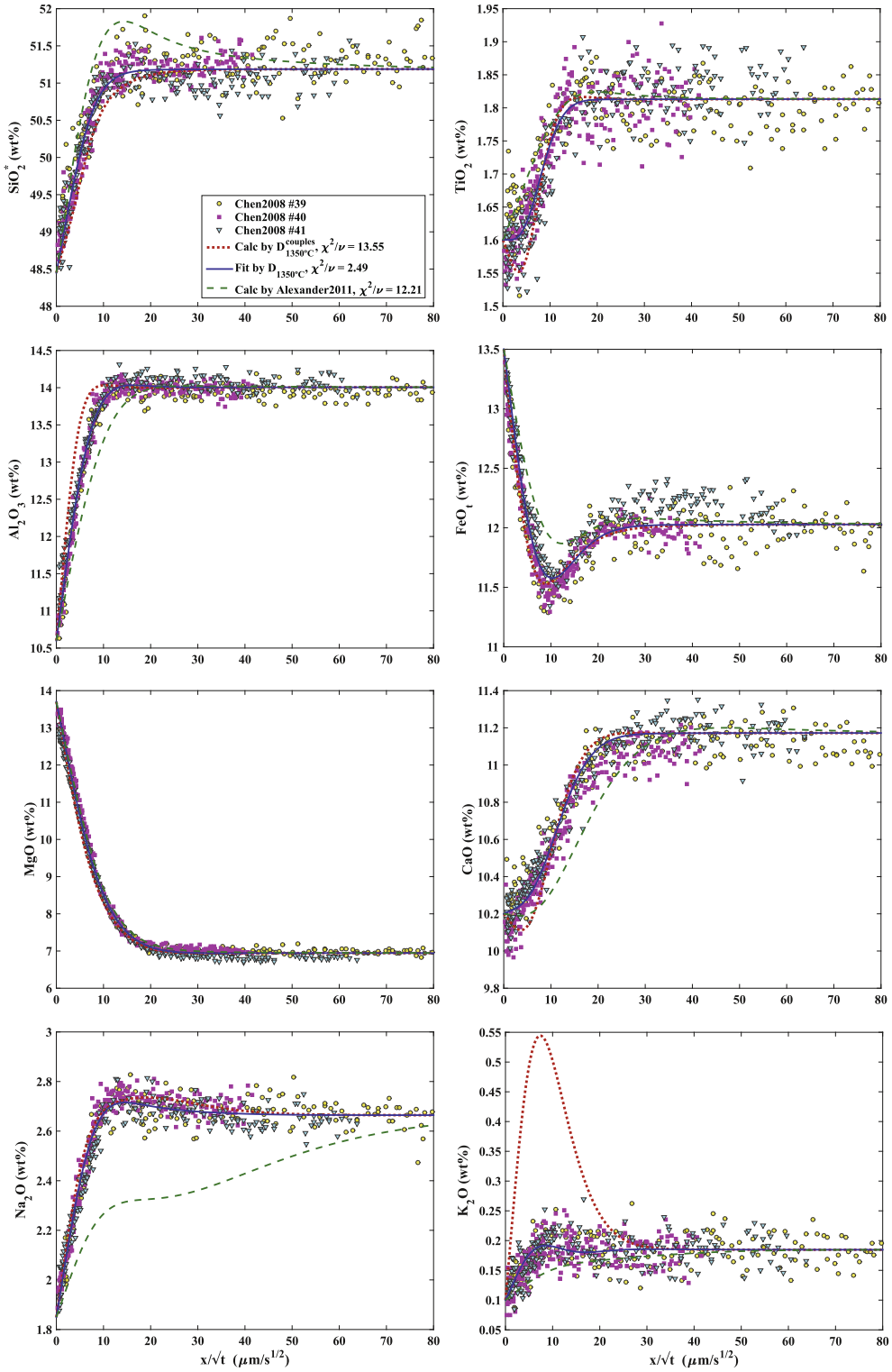

Fig. 3. Predicted and fit diffusion profiles for olivine dissolution in basaltic melts at ~1350 °C (Chen and Zhang, 2008). The long-dashed green curves are predicted profiles using the diffusion matrix given by Alexander 2011 (Note this diffusion matrix was corrected to 1350 °C for comparison). The short-dashed red curves are predicted profiles using the diffusion matrix $D^{couples}_{1350°C}$ in Table 4. The solid curves are fit profiles for obtaining the diffusion matrix $D_{1350°C}$ in Table 5. χ^2/ν is calculated and shown for each component.

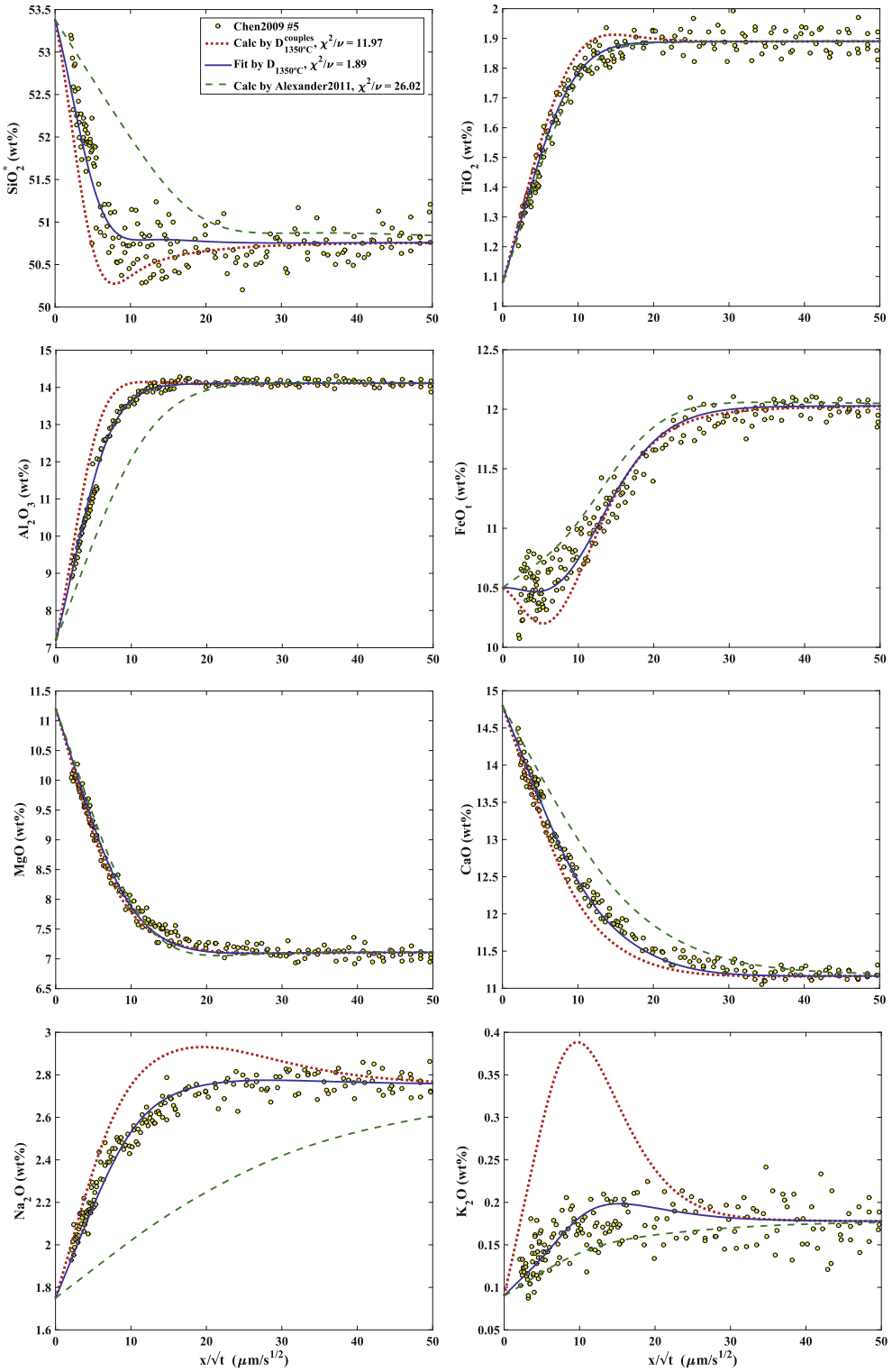

Fig. 4. Predicted and fit diffusion profiles for diopside dissolution in basaltic melts at ~1350 °C (Chen and Zhang, 2009). The long-dashed green curves are predicted profiles using the diffusion matrix given by Alexander 2011 (Note this diffusion matrix was corrected to 1350 °C for comparison). The short-dashed red curves are predicted profiles using the diffusion matrix $D^{couples}_{1350°C}$ in Table 4. The solid curves are fit profiles for obtaining the diffusion matrix $D_{1350°C}$ in Table 5. χ^2/ν is calculated and shown for each component.

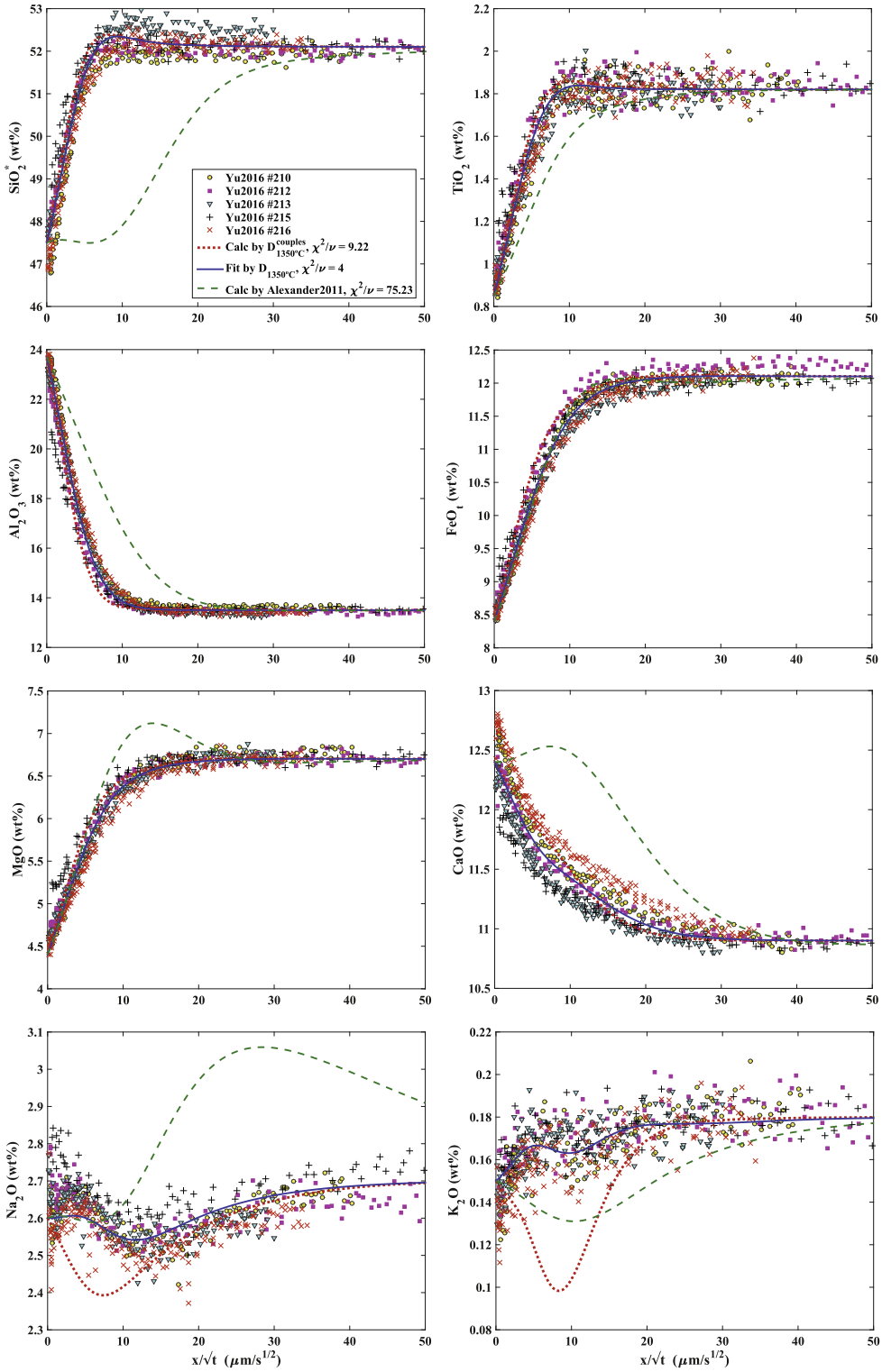

Fig. 5. Predicted and fit diffusion profiles for anorthite dissolution in basaltic melts at ~1350 °C (Yu et al., 2016). The long-dashed green curves are predicted profiles using the diffusion matrix given by Alexander 2011 (Note this diffusion matrix was corrected to 1350 °C for comparison). The short-dashed red curves are predicted profiles using the diffusion matrix $D^{couples}_{1350°C}$ in Table 4. The solid curves are fit profiles for obtaining the diffusion matrix $D_{1350°C}$ in Table 5. χ^2/ν is calculated and shown for each component.

Table 5
Diffusion matrix $D_{1350°C}$, obtained by fitting both the 9 diffusion couple experiments and mineral dissolution experiments at ~1350 °C, with 1σ errors for each element, and eigenvalues and eigenvectors.

$D_{1350°C}$ ($\mu m^2/s$)	TiO_2	Al_2O_3	FeO	MgO	CaO	Na_2O	K_2O
TiO_2	7.81 ± 0.32	–0.25 ± 0.07	–1.53 ± 0.23	–2.02 ± 0.31	–2.76 ± 0.46	–6.43 ± 1.67	–3.17 ± 0.72
Al_2O_3	–0.81 ± 0.70	5.69 ± 0.14	–7.85 ± 0.43	–6.77 ± 0.55	–14.96 ± 0.82	–29.73 ± 2.90	–20.57 ± 1.43
FeO	–21.66 ± 1.30	–3.70 ± 0.27	23.21 ± 0.91	–31.24 ± 1.08	–38.91 ± 1.57	–72.85 ± 5.73	–46.15 ± 2.48
MgO	–5.52 ± 0.73	1.11 ± 0.16	–7.93 ± 0.55	27.21 ± 0.64	–21.46 ± 0.90	–39.21 ± 3.11	–7.33 ± 1.54
CaO	13.58 ± 1.48	–4.62 ± 0.21	–17.94 ± 0.69	–8.93 ± 0.80	37.88 ± 1.16	–38.15 ± 4.14	15.44 ± 1.66
Na_2O	19.68 ± 1.90	10.28 ± 0.29	28.83 ± 0.90	39.57 ± 0.87	57.21 ± 1.31	243.78 ± 4.65	77.02 ± 1.74
K_2O	5.54 ± 0.33	1.42 ± 0.07	3.24 ± 0.19	4.47 ± 0.28	8.47 ± 0.44	21.37 ± 1.51	39.83 ± 0.73
Eigenvalues	λ_1	λ_2	λ_3	λ_4	λ_5	λ_6	λ_7
	6.43						
		8.18					
			14.95				
				31.43			
					41.68		
						58.24	
							224.52
Eigenvectors	v_1	v_2	v_3	v_4	v_5	v_6	v_7
SiO_2	–0.73	0.86	–0.22	–0.41	–0.04	0.05	–0.27
TiO_2	0.03	–0.28	–0.16	–0.02	–0.01	–0.01	–0.02
Al_2O_3	0.68	–0.23	–0.63	–0.23	–0.13	–0.08	–0.10
FeO	0.05	–0.23	0.54	0.76	0.51	–0.42	–0.29
MgO	–0.03	–0.14	0.36	–0.22	–0.75	–0.30	–0.15
CaO	0.07	–0.19	0.30	–0.08	0.39	0.84	–0.14
Na_2O	–0.04	0.09	–0.15	–0.16	–0.06	–0.15	0.89
K_2O	–0.03	0.13	–0.04	0.35	0.08	0.06	0.09

See footnote on Table 4 for the expression of each eigenvector in 8–component space.

Eigenvalues and eigenvectors of the diffusion matrix $D_{1350°C}$ are shown in Table 5. By examining eigenvectors of matrix $D_{1350°C}$ (Table 5), the eigenvectors are similar to those for $D^{couples}_{1350°C}$: for example, v_1 is largely due to the exchange between SiO_2 and Al_2O_3; and v_7 is due to the exchange of Na_2O (and very minor K_2O) with all other components.

The diffusion mechanism during multicomponent diffusion in basaltic melts is summarized in Table 6. One may classify it into 5 categories: (1) the exchange between network-formers, such as SiO_2 – Al_2O_3; (2) the exchange between divalent network-modifiers and all other components, such as (FeO + MgO + CaO) – (all others); (3) the exchange of divalent plus monovalent network-modifier with all other components, such as (FeO + K_2O) – (all others) and (CaO + K_2O) – (all others); (4) the exchange between divalent network-modifiers, such as (FeO + CaO) – MgO; and (5) the exchange of monovalent network-modifier Na_2O with all other components. Curiously, diffusion of K_2O does not dominate any diffusion eigenvector.

Because combining mineral dissolution experiments with diffusion couple experiments improves the accuracy and predictive power of the diffusion matrix, we applied the method to our earlier data (Guo and Zhang, 2016) on the 7-component SiO_2–TiO_2–Al_2O_3–MgO–CaO–Na_2O–K_2O system at 1500 °C to obtain a more accurate diffusion matrix (Table 7), with new fits in the supplementary files (Figs. S11–S20). This new diffusion matrix is preferred over the diffusion matrix in Guo and Zhang (2016).

Table 6
Multicomponent diffusion mechanism in basaltic melts at 1350 °C.

Sequence	Eigenvalues	Eigenvectors	Exchanging species at 1350 °C
Slowest	λ_1	v_1	SiO_2 – Al_2O_3
2nd slowest	λ_2	v_2	SiO_2 – (all others)
3rd slowest	λ_3	v_3	(FeO + MgO + CaO) – (all others)
4th fastest	λ_4	v_4	(FeO + K_2O) – (all others)
3rd fastest	λ_5	v_5	(FeO + CaO) – MgO
2nd fastest	λ_6	v_6	(CaO + K_2O) – (all others)
Fastest	λ_7	v_7	Na_2O – (all others)

Table 7
Diffusion matrix for the 7–component haplobasaltic melt (Guo and Zhang, 2016) obtained by fitting both the 9 diffusion couple experiments and an anorthite dissolution experiment at ~1500 °C, with 1σ errors for each element, and eigenvalues and eigenvectors.

D ($\mu m^2/s$)	TiO_2	Al_2O_3	MgO	CaO	Na_2O	K_2O
TiO_2	18.78 ± 0.36	–0.81 ± 0.53	–4.20 ± 0.62	–11.10 ± 1.26	–27.13 ± 2.96	–15.54 ± 3.60
Al_2O_3	–4.72 ± 0.99	8.96 ± 1.00	–17.40 ± 1.23	–36.01 ± 2.03	–60.32 ± 4.81	–80.65 ± 5.58
MgO	–6.77 ± 1.18	0.22 ± 1.15	39.02 ± 1.68	–39.62 ± 2.47	–82.61 ± 5.57	–45.38 ± 7.35
CaO	–11.20 ± 1.37	–4.56 ± 1.53	–27.62 ± 1.75	64.89 ± 2.69	–31.03 ± 5.60	30.37 ± 7.88
Na_2O	27.40 ± 1.29	11.66 ± 1.44	48.66 ± 1.67	59.90 ± 1.89	341.56 ± 3.97	98.05 ± 6.37
K_2O	5.39 ± 0.53	5.98 ± 0.49	11.67 ± 0.64	15.20 ± 0.98	–0.37 ± 1.94	114.29 ± 2.61
Eigenvalues	λ_1	λ_2	λ_3	λ_4	λ_5	λ_6
	13.73					
		19.88				
			35.59			
				80.95		
					122.02	
						315.33
Eigenvectors	v_1	v_2	v_3	v_4	v_5	v_6
TiO_2	–0.03	0.90	0.15	0.06	0.05	–0.08
Al_2O_3	0.99	–0.20	0.35	0.09	0.37	–0.15
MgO	–0.07	0.18	–0.69	0.57	0.27	–0.26
CaO	0.07	0.30	–0.58	–0.80	–0.63	–0.09
Na_2O	–0.02	–0.12	0.14	0.01	0.33	0.95
K_2O	–0.06	–0.11	0.18	0.14	–0.54	–0.03

9. COMPARISON WITH PREVIOUS WORKS

There are no other diffusion matrices for 8-component system in the literature. Hence, no direct comparison between the diffusion matrix (Table 5) from this study and that in the literature can be made. There are diffusion matrices in simpler systems, but they are at different temperatures. Therefore, no comparison can be made by crossing out rows and columns of the diffusion matrix (Table 5) for our 8-component system. Nonetheless, diffusion mechanisms inferred from eigenvectors can be compared.

In general, diffusion matrices in simpler component systems indicate that the exchange between network-former SiO_2 and Al_2O_3 is the slowest for any SiO_2–Al_2O_3 bearing systems (Sugawara et al. 1977; Oishi et al., 1982; Chakraborty et al., 1995; Kress and Ghiorso, 1995; Liang et al., 1996; Mungall et al., 1998; Richter et al., 1998; Liang and Davis, 2002; Liang, 2010; Guo and Zhang, 2016) and the exchange between Na_2O and other components is the fastest for Na_2O-bearing system (Watkins et al., 2014; Claireaux et al., 2016; Guo and Zhang, 2016). These are consistent with our results.

For Na_2O-absent systems, diffusion matrix in 4-component SiO_2–Al_2O_3–MgO–CaO systems reported by Liang (2010) indicates that the fastest diffusion is due to the exchange of CaO with all other components, and diffusion matrix in SiO_2–TiO_2–Al_2O_3–FeO–MgO–CaO reported by Kress and Ghiorso (1995) indicates the fastest diffusion corresponds to the exchange between divalent cations FeO, MgO and CaO, both of which are consistent with our findings if only SiO_2, Al_2O_3, FeO, MgO and CaO components are considered.

Furthermore, Guo and Zhang (2016) reported a diffusion matrix for 7-component SiO_2–TiO_2–Al_2O_3–MgO–CaO–Na_2O–K_2O system. Their inferred diffusion mechanism is that the slowest diffusion is largely due to the exchange between network-former SiO_2 and Al_2O_3, the second slowest diffusion is largely due to the exchange between SiO_2 and TiO_2, the third slowest diffusion is due to the exchange of network-former $SiO_2 + Al_2O_3$ with divalent network-modifier MgO + CaO, the third fastest diffusion is largely due to the exchange between divalent network-modifier MgO and CaO, the second fastest diffusion is due to the exchange of CaO + K_2O with all other components, and the fastest diffusion is largely due to the exchange of monovalent Na_2O with all other components. This is very consistent with the diffusion mechanism found in this study, if FeO component is ignored in Table 6.

However, there are also exceptions: In the 4-component SiO_2-Al_2O_3-CaO-Na_2O system, Claireaux et al. (2016) found that the slowest diffusion eigenvector is predominantly due to the exchange between Al_2O_3 and CaO, rather than between SiO_2 and Al_2O_3. In Columbia River basalt modeled as a 6-component SiO_2–TiO_2–Al_2O_3–FeO–MgO–CaO system, Kress and Ghiorso (1995) obtained that the slowest diffusion eigenvector is mainly due to SiO_2 exchange with FeO + CaO at 1200 °C, and due to Al_2O_3 exchange with MgO at 1300 °C. It is not clear what caused the differences.

In summary, there is an overall agreement among different studies on diffusion mechanism, but inconsistencies are also present. The explanation for the inconsistencies is not readily available, but uncertainty in the diffusion matrix and differences in composition and temperature are possible contributing factors.

10. SUMMARY AND CONCLUSIONS

Chemical diffusion profiles of 9 successful diffusion couple experiments at ~1350 °C and at 1 GPa, in basaltic melts in an 8-component SiO_2–TiO_2–Al_2O_3–FeO–MgO–CaO–Na_2O–K_2O system were determined. Effective binary diffusion coefficients of components with monotonic diffusion profiles at ~1350 °C show a strong dependence on its counter-diffusing component. Multicomponent diffusion matrix in basaltic melts was obtained in two ways: (1) by simultaneously fitting diffusion profiles of 9 diffusion couple experiments in this study, and (2) by simultaneously fitting diffusion profiles of both diffusion couple experiments in this study and mineral dissolution experiments in the literature. The two diffusion matrices are similar, showing the robustness of the results. Furthermore, 9 diffusion couple experiments are enough for the extraction of diffusion matrix in an 8-component system. Nonetheless, when mineral dissolution data are used in the fitting, the obtained diffusion matrix can predict diffusion profiles during mineral dissolution experiments much better. Diffusion mechanism inferred from eigenvectors of the diffusion matrix is reasonable and consistent with previous studies by Liang (2010) and Guo and Zhang (2016).

ACKNOWLEDGEMENT

Constructive reviews by Michael Toplis, Yan Liang and Emmanuelle Gouillart are highly appreciated. We thank Peng Ni for helping us analyze XANES. This research is supported by NSF grant EAR-1524473. The electron microprobe Cameca SX100 used in this study was purchased using NSF grant EAR-9911352.

APPENDIX A. SUPPLEMENTARY MATERIAL

Supplementary data associated with this article can be found, in the online version, at https://doi.org/10.1016/j.gca.2018.02.043.

REFERENCES

Alexander C. M. (2011) Modeling diffusive dissolution in silicate melts. *Geochim. Cosmochim. Acta* **75**, 588–607.

Asimow P. D. and Ghiorso M. S. (1998) Algorithmic modifications extending MELTS to calculate subsolidus phase relations. *Am. Mineral.* **83**, 1127–1131.

Chakraborty S., Dingwell D. B. and Rubie D. C. (1995) Multicomponent diffusion in ternary silicate melts in the system K_2O–Al_2O_3–SiO_2: I. Experimental measurements. *Geochim. Cosmochim. Acta* **59**, 255–264.

Chen Y. and Zhang Y. (2008) Olivine dissolution in basaltic melt. *Geochim. Cosmochim. Acta* **72**, 4756–4777.

Chen Y. and Zhang Y. (2009) Clinodiopside dissolution in basaltic melt. *Geochim. Cosmochim. Acta* **73**, 5730–5747.

Claireaux C., Chopinet M., Burov E., Gouillart E., Roskosz M. and Toplis M. (2016) Atomic mobility in calcium and sodium aluminosilicate melts at 1200 °C. *Geochim. Cosmochim. Acta* **192**, 235–247.

Clifford A. A. (1973) *Multivariate Error Analysis: A Handbook of Error Propagation and Calculation in Many-Parameter System*. Wiley, NY.

Cooper A. R. (1968) The use and limitations of the concept of an effective binary diffusion coefficient for multi-component diffusions. In *Mass Transport In Oxides*, vol. 296 (eds. J. B. Wachman and A. D. Franklin). Nat. Bur. Stand. Spec. Publ, pp. 79–84.

Dixon J. E., Clague D. A. and Eissen J. P. (1986) Gabbroic xenoliths and host ferrobasalt from the Southern Juan de Fuca Ridge. *J. Geophys. Res.* **91**, 3795–3820.

Dixon J. E., Stolper E. and Delaney J. R. (1988) Infrared spectroscopic measurements of CO_2 and H_2O in Juan de Fuca Ridge basaltic glasses. *Earth Planet. Sci. Lett.* **90**, 87–104.

Fletcher, R., 1971. A modified Marquardt subroutine for nonlinear least squares. Atomic Energy Research Establishment R6799, Harwell, England.

Ghiorso M. S. and Sack R. O. (1995) Chemical mass transfer in magmatic processes IV. A revised and internally consistent thermodynamic model for the interpolation and extrapolation of liquid–solid equilibria in magmatic systems at elevated temperatures and pressures. *Contrib. Mineral. Petrol.* **119**, 197–212.

Guo C. and Zhang Y. (2016) Multicomponent diffusion in silicate melts: SiO_2–TiO_2–Al_2O_3–FeO–MgO–CaO–Na_2O–K_2O system. *Geochim. Cosmochim. Acta* **195**, 126–141.

Hui H., Zhang Y. and Behrens H. (2008) Pressure dependence of the speciation of dissolved water in rhyolitic melts. *Geochim. Cosmochim. Acta* **72**, 3229–3240.

Koyaguchi T. (1985) Magma mixing in a conduit. *J. Volcanol. Geotherm. Res.* **25**, 365–369.

Koyaguchi T. (1989) Chemical gradient at diffusive interfaces in magma chambers. *Contrib. Mineral. Petrol.* **103**, 143–152.

Kress V. C. and Ghiorso M. S. (1993) Multicomponent diffusion in MgO–Al_2O_3–SiO_2 and Cao–MgO–Al_2O_3–SiO_2 melts. *Geochim. Cosmochim. Acta* **57**, 4453–4466.

Kress V. C. and Ghiorso M. S. (1995) Multicomponent diffusion in basaltic melts. *Geochim. Cosmochim. Acta* **59**, 313–324.

Lange R. L. and Carmichael I. S. E. (1990) Thermodynamic properties of silicate liquids with emphasis on density, thermal expansion and compressibility. *Rev. Mineral. Geochem.* **24**, 25–64.

Lasaga A. C. (1979) Multicomponent exchange and diffusion in silicates. *Geochim. Cosmochim. Acta* **54**, 2709–2715.

Liang Y. (2010) Multicomponent diffusion in molten silicates: theory, experiments, and geological application. *Rev. Mineral. Geochem.* **72**, 409–446.

Liang Y. and Davis A. M. (2002) Energetics of multicomponent diffusion in molten CaO–Al_2O_3–SiO_2. *Geochim. Cosmochim. Acta* **66**, 635–646.

Liang Y., Richter F. M. and Chamberlin L. (1997) Diffusion in silicate melts: III. Empirical models for multicomponent diffusion. *Geochim. Cosmochim. Acta* **61**, 5295–5312.

Liang Y., Richter F. M. and Watson E. B. (1994) Convection in multicomponent silicate melts driven by coupled diffusion. *Nature* **369**, 390–392.

Liang Y., Richter F. M. and Watson E. B. (1996) Diffusion in silicate melts: II. Multicomponent diffusion in CaO–SiO_2–Al_2O_3 at 1500°C and 1GPa. *Geochim. Cosmochim. Acta* **60**, 5021–5035.

Morgan Z. T., Liang Y. and Hess P. C. (2006) An experimental study of the kinetics of anorthite dissolution in lunar picritic magmas with applications to lunar crustal assimilation processes. *Geochim. Cosmochim. Acta* **70**, 3477–3491.

Mungall J. E., Romano C. and Dingwel D. B. (1998) Multicomponent diffusion in the molten system K_2O–Na_2O–Al_2O_3–SiO_2–H_2O. *Am. Mineral.* **83**, 685–699.

Ni H. and Zhang Y. (2008) H_2O diffusion models in rhyolitic melt with new high pressure data. *Chem. Geol.* **250**, 68–78.

Oishi Y., Nanba M. and Pask J. A. (1982) Analysis of liquid–state interdiffusion in the system $CaO–Al_2O_3–SiO_2$ using multiatomic ion models. *J. Am. Ceram. Soc.* **65**, 247–253.

Oldenburg C. M., Spera F. J., Yuen D. A. and Sewell G. (1989) Dynamic mixing in magma bodies: theory, simulations and implications. *J. Geophys. Res.* **94**, 9215–9236.

Pablo H., Schuller S., Toplis M. J., Gouillart E., Mostefaoui S., Charpentier T. and Roskosz M. (2017) Multicomponent diffusion in sodium borosilicate glasses. *J. Non-Cryst. Solids* **478**, 20–40.

Richter F. M. (1993) A method for determining activity–composition relations using chemical diffusion in silicate melts. *Geochim. Cosmochim. Acta* **57**, 2019–2032.

Richter F. M., Liang Y. and Minarik W. G. (1998) Multicomponent diffusion and convection in molten $MgO–Al_2O_3–SiO_2$. *Geochim. Cosmochim. Acta* **62**, 1985–1991.

Sato H. (1975) Diffusion coronas around quartz xenocrysts in andesite and basalt from Tertiary Volcanic Region in northeastern Shikoku, Japan. *Contrib. Mineral. Petrol.* **50**, 49–64.

Sugawara H., Nagata K. and Goto K. S. (1977) Interdiffusivities matrix of $CaO–Al_2O_3–SiO_2$ melt at 1723 K to 1823 K. *Metall. Trans. B* **8**, 605–612.

Trial A. F. and Spera F. J. (1994) Measuring the multicomponent diffusion matrix: experimental design and data analysis for silicate melts. *Geochim. Cosmochim. Acta* **58**, 3769–3783.

Turner J. S. (1985) Multicomponent convection. *Ann. Rev. Fluid Mech.* **17**, 11–44.

Watson E. B. (1982) Basalt contamination by continental crust: Some experiments and models. *Contrib. Mineral. Petrol.* **80**, 73–87.

Watkins J. M., Liang Y., Richter F., Ryerson F. J. and DePaolo D. J. (2014) Diffusion of multi-isotopic chemical species in molten silicates. *Geochim. Cosmochim. Acta* **139**, 313–326.

Yu Y., Zhang Y., Chen Y. and Xu Z. (2016) Kinetics of anorthite dissolution in basaltic melt. *Geochim. Cosmochim. Acta* **179**, 257–274.

Zhang Y. (1993) A modified effective binary diffusion model. *J. Geophys. Res.* **98**, 11901–11920.

Zhang Y. and Behrens H. (2000) H_2O diffusion in rhyolitic melts and glasses. *Chem. Geol.* **169**, 243–262.

Zhang Y., Ni H. and Chen Y. (2010) Diffusion data in silicate melts. *Rev. Mineral. Geochem.* **72**, 311–408.

Zhang Y., Walker D. and Lesher C. E. (1989) Diffusive crystal dissolution. *Contrib. Mineral. Petrol.* **102**, 492–513.

Associate editor: Michael J. Toplis

SUPPLEMENTARY FILE

1. Electron microprobe analysis conditions

Table S1. Electron microprobe analysis conditions

spectrometer	element	Xtal	position	background+	background–	counting time
Sp1	Na	LTAP	~46381	–1400	820	30s
Sp1	Si	LTAP	~27747	–560	980	30s
Sp2	Mg	TAP	~38505	–1600	1000	30s
Sp2	Al	TAP	~32449	–850	850	30s
Sp3	K	LPET	~42752	–530	1100	30s
Sp3	Ca	LPET	~38381	–700	1300	30s
Sp4	Ti	LLIF	~68278	–620	1380	30s
Sp4	Fe	LLIF	~48084	–1200	1250	30s

Note: Multiple-period-counting sequence of elements in each spectrometer is the same sequence listed in the table. Peak positions change slightly for each analysis. No Na-loss was observed, so time-0 intercept was not used.

2. Test whether matrices $D_{1350°C}^{couples}$ and $D_{1350°C}$ are significantly different

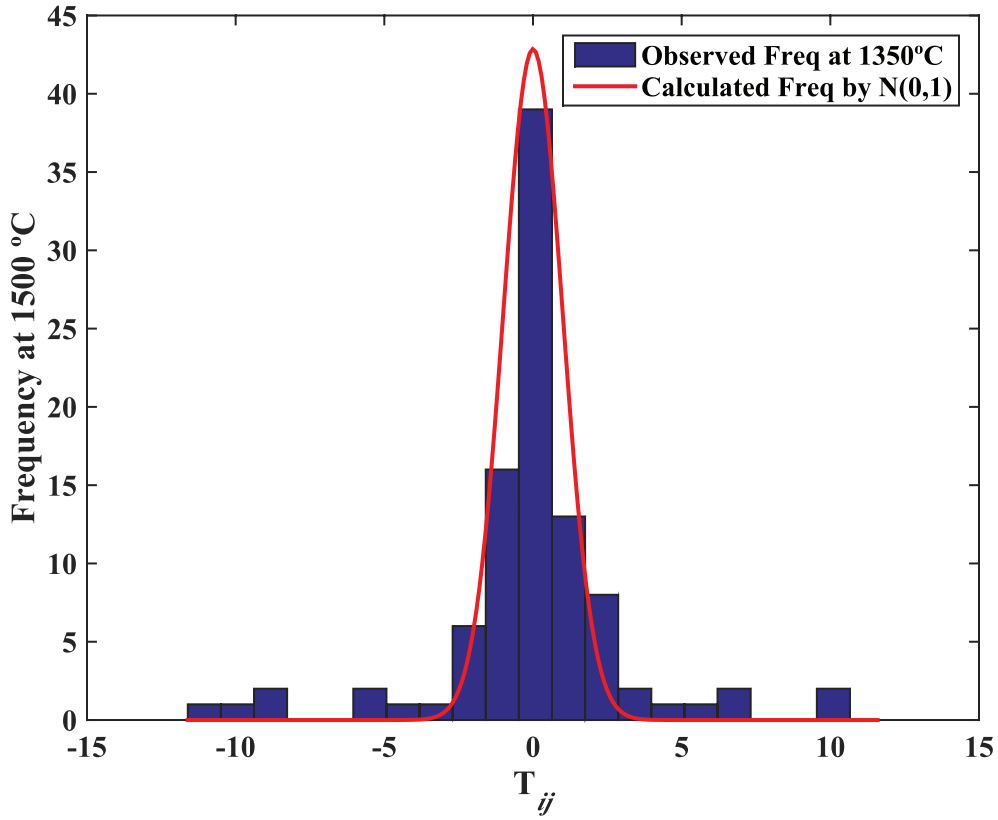

Fig. S1. Comparison between observed frequency and calculated frequency from a standard normal distribution.

3. All predictions and fits for 9 diffusion couple experiments at 1350 ºC

All the points represent the measured data, and the different styles of the symbols indicate different traverses. All the predictions by the diffusion matrix (Note this diffusion matrix was corrected to 1350 ºC for comparison) given by Alexander (2011) for all 9 diffusion couple experiments are shown by long-dashed curves in Figs. S2–S10. All the fits for all 9 diffusion couple experiments by diffusion matrix $D^{couples}_{1350ºC}$ in Table 4 are shown by short-dashed curves in Figs. S2–S10. All the fits for all 9 diffusion couple experiments by diffusion matrix $D_{1350ºC}$ in Table 5 are shown by solid curves in Figs. S2–S10.

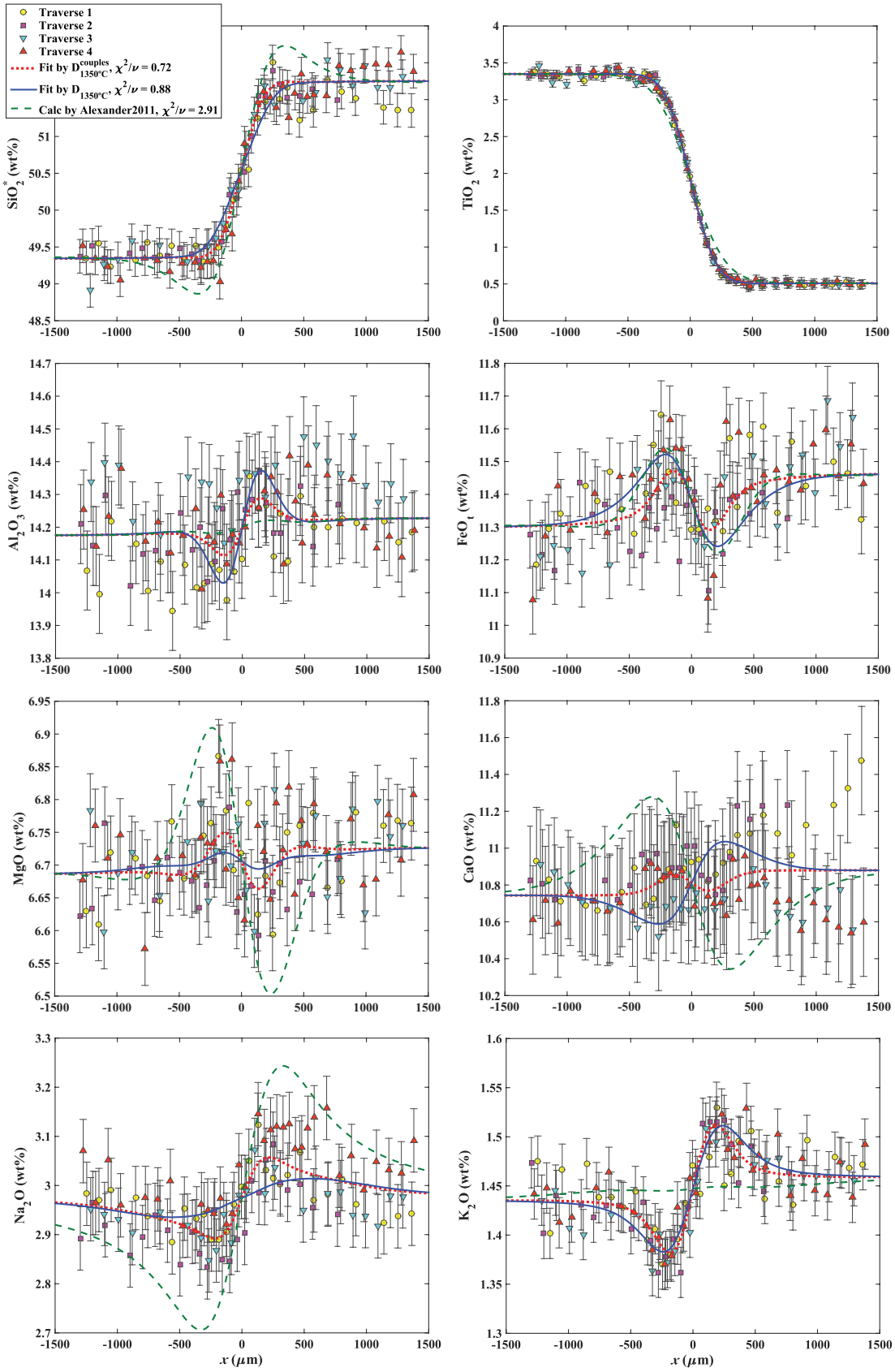

Fig. S2. Diffusion profiles of diffusion couple BS1&2A with predictions by diffusion matrix given by Alexander (2011) and fits by diffusion matrices $D^{couples}_{1350°C}$ in Table 4 and $D_{1350°C}$ in Table 5.

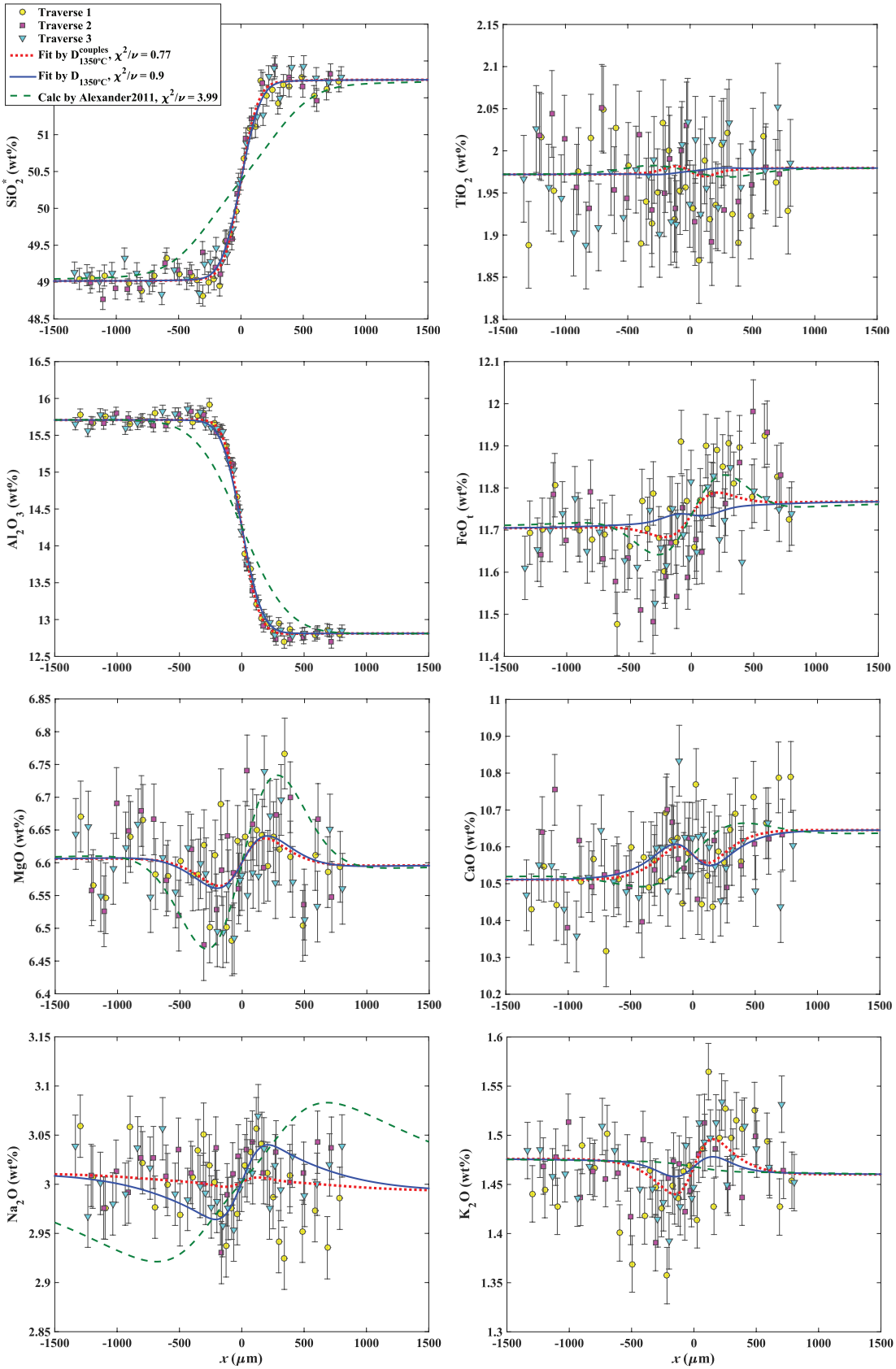

Fig. S3. Diffusion profiles of diffusion couple BS3&4A with predictions by diffusion matrix given by Alexander (2011) and fits by diffusion matrices $D^{couples}_{1350°C}$ in Table 4 and $D_{1350°C}$ in Table 5.

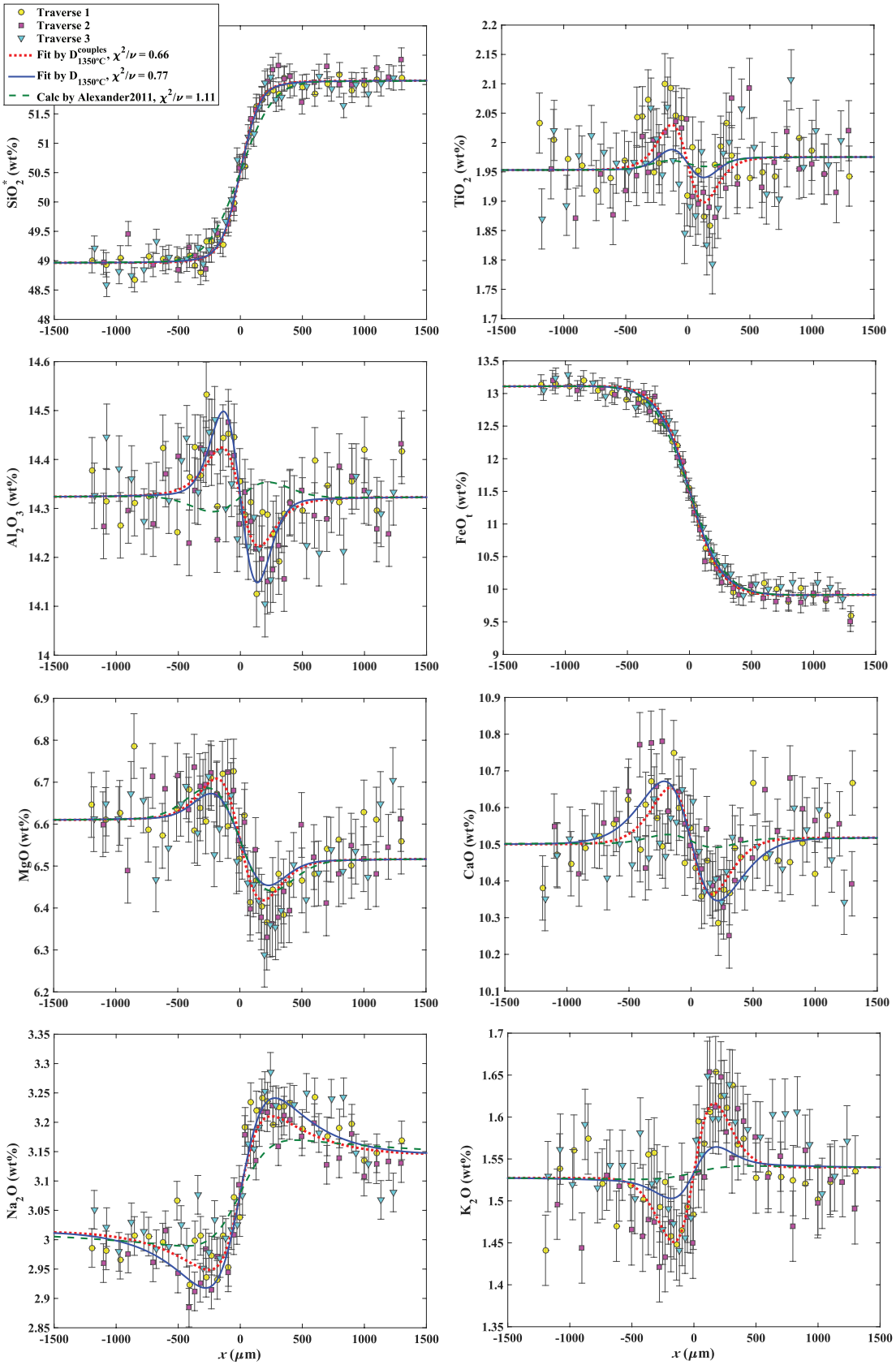

Fig. S4. Diffusion profiles of diffusion couple BS5&6A with predictions by diffusion matrix given by Alexander (2011) and fits by diffusion matrices $D^{couples}_{1350°C}$ in Table 4 and $D_{1350°C}$ in Table 5.

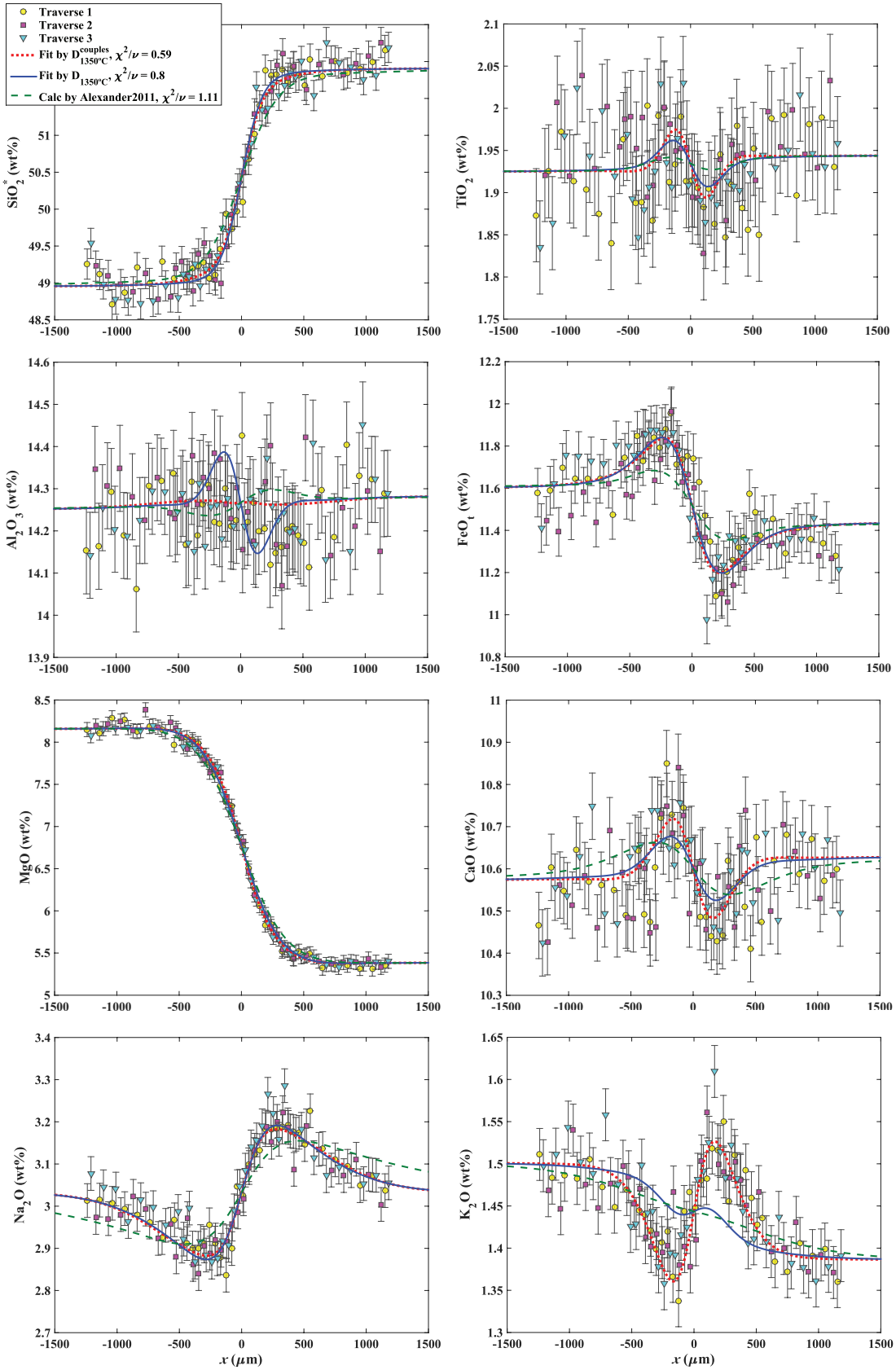

Fig. S5. Diffusion profiles of diffusion couple BS7&8A with predictions by diffusion matrix given by Alexander (2011) and fits by diffusion matrices $D^{couples}_{1350°C}$ in Table 4 and $D_{1350°C}$ in Table 5.

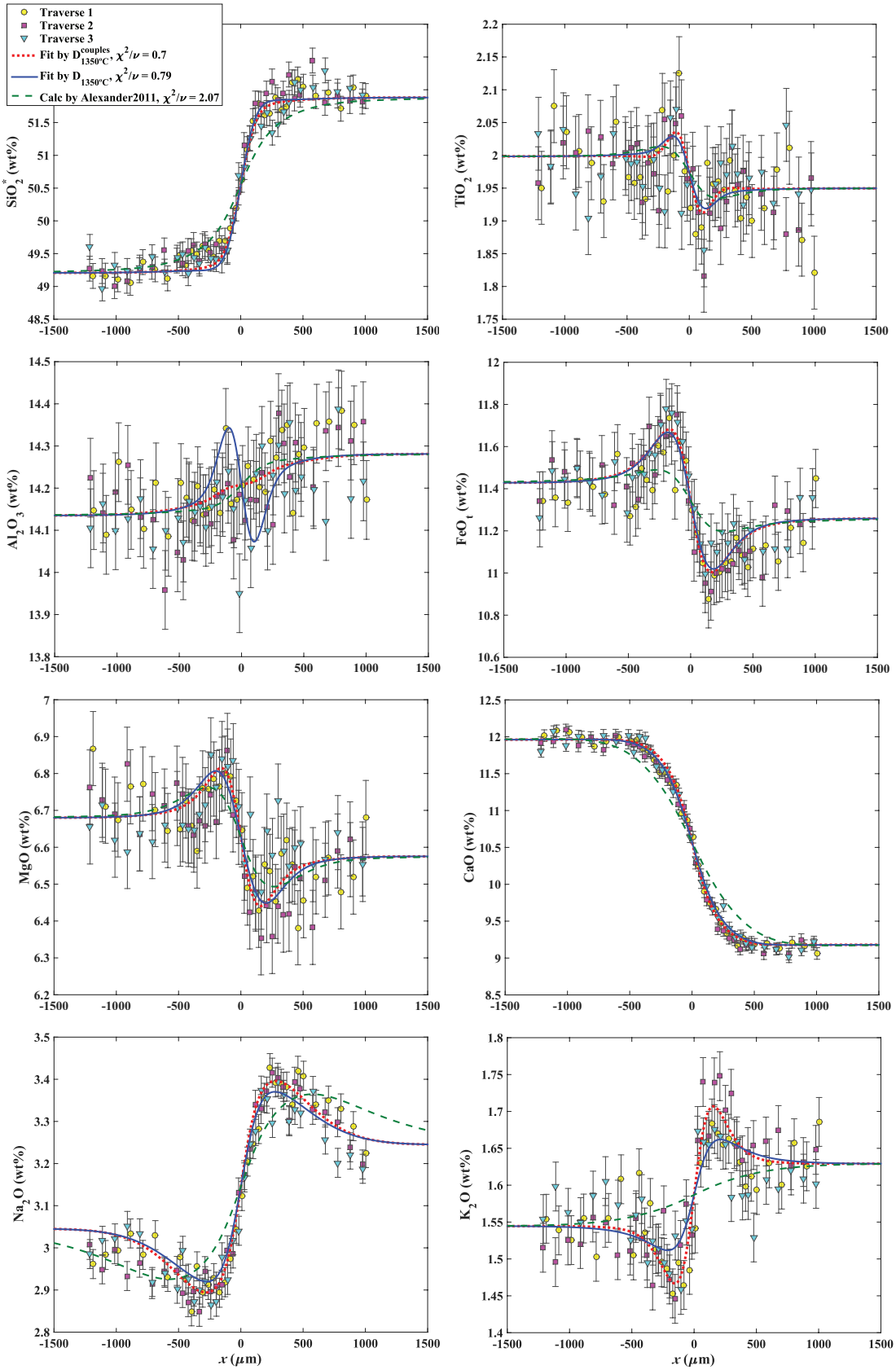

Fig. S6. Diffusion profiles of diffusion couple BS9&10A with predictions by diffusion matrix given by Alexander (2011) and fits by diffusion matrices $D^{couples}_{1350°C}$ in Table 4 and $D_{1350°C}$ in Table 5.

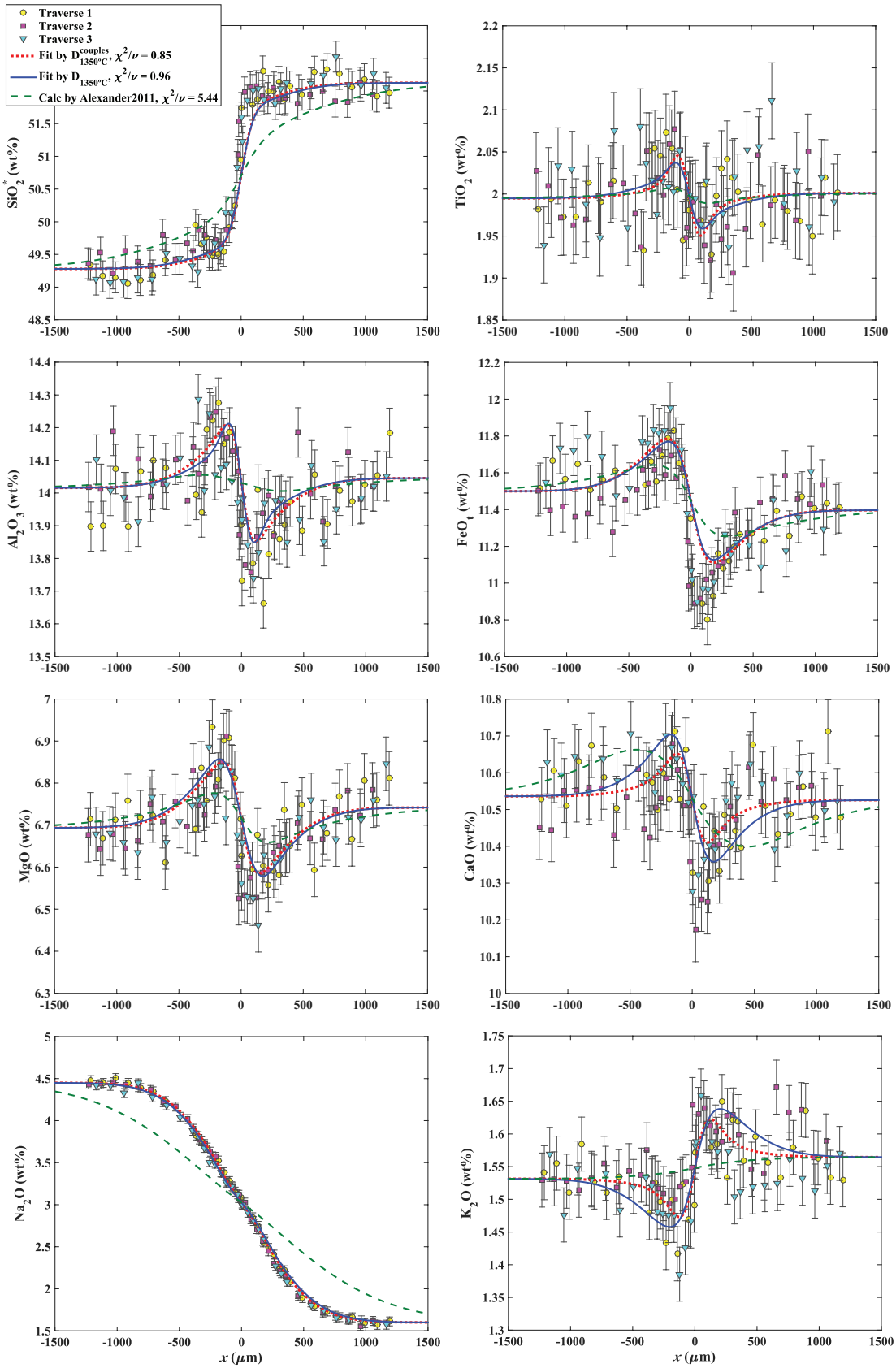

Fig. S7. Diffusion profiles of diffusion couple BS11&12A with predictions by diffusion matrix given by Alexander (2011) and fits by diffusion matrices $D^{couples}_{1350°C}$ in Table 4 and $D_{1350°C}$ in Table 5.

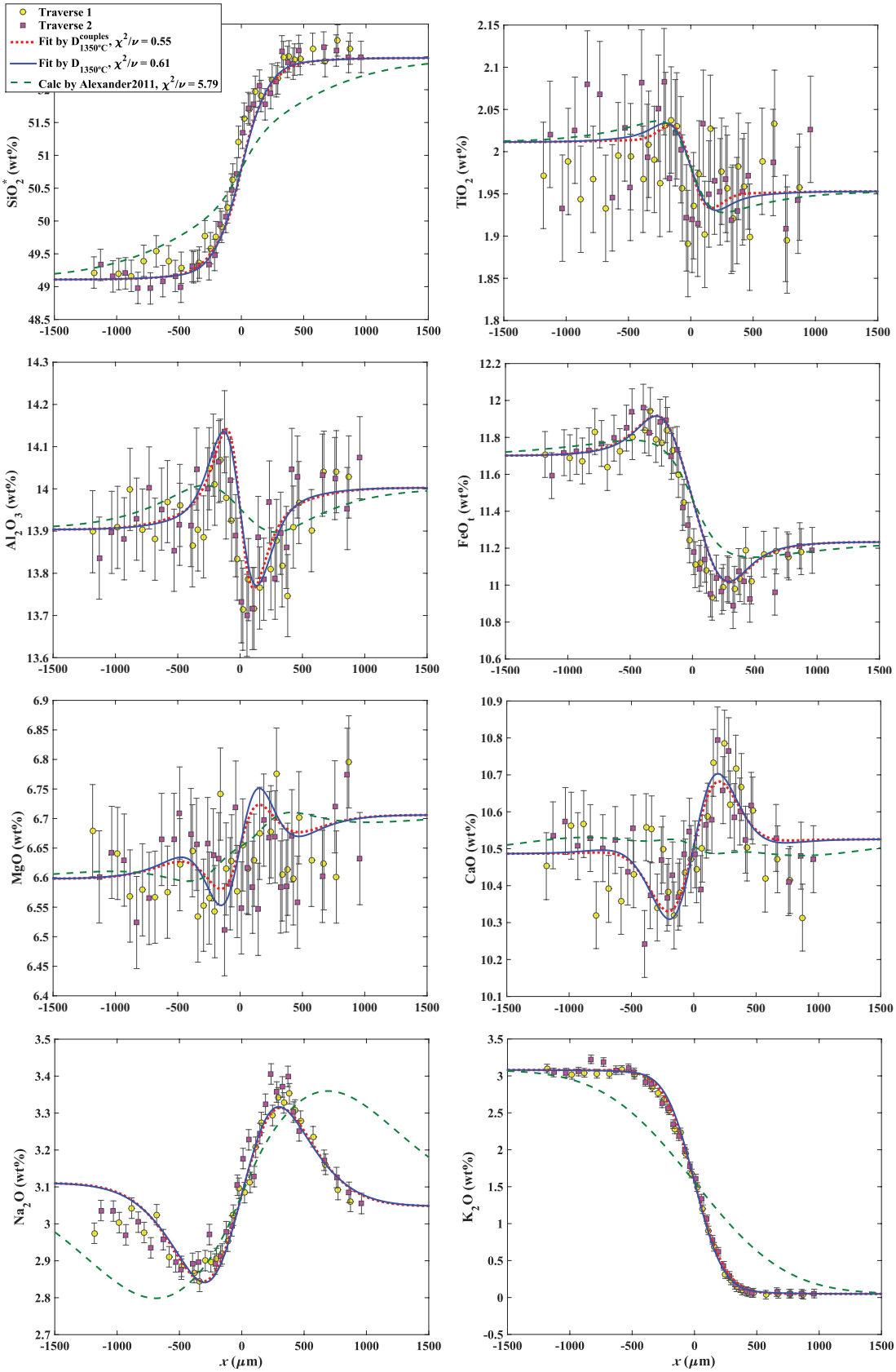

Fig. S8. Diffusion profiles of diffusion couple BS13&14A with predictions by diffusion matrix given by Alexander (2011) and fits by diffusion matrices $D^{couples}_{1350°C}$ in Table 4 and $D_{1350°C}$ in Table 5.

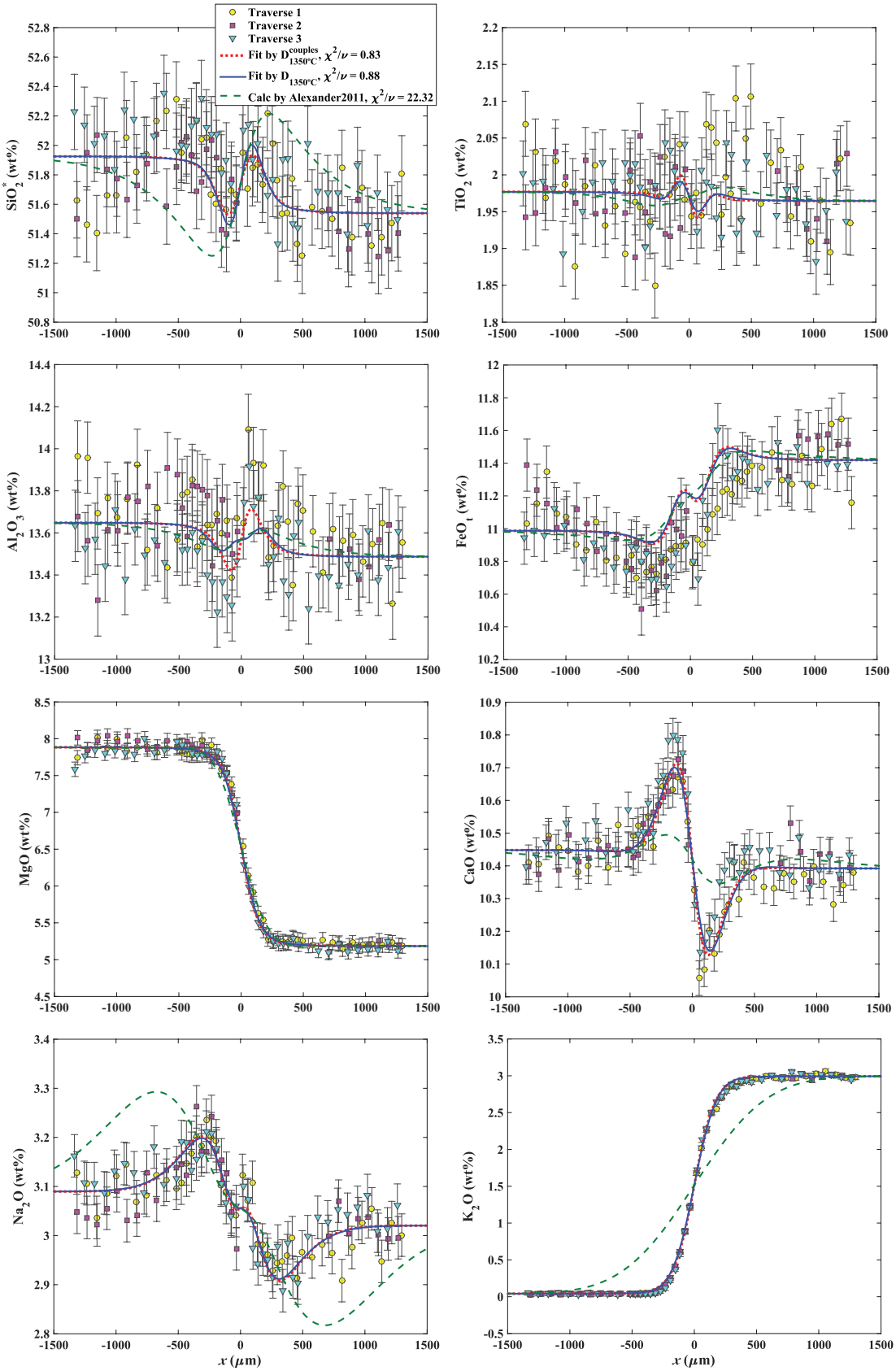

Fig. S9. Diffusion profiles of diffusion couple BS17&18A with predictions by diffusion matrix given by Alexander (2011) and fits by diffusion matrices $D^{\text{couples}}_{1350°C}$ in Table 4 and $D_{1350°C}$ in Table 5.

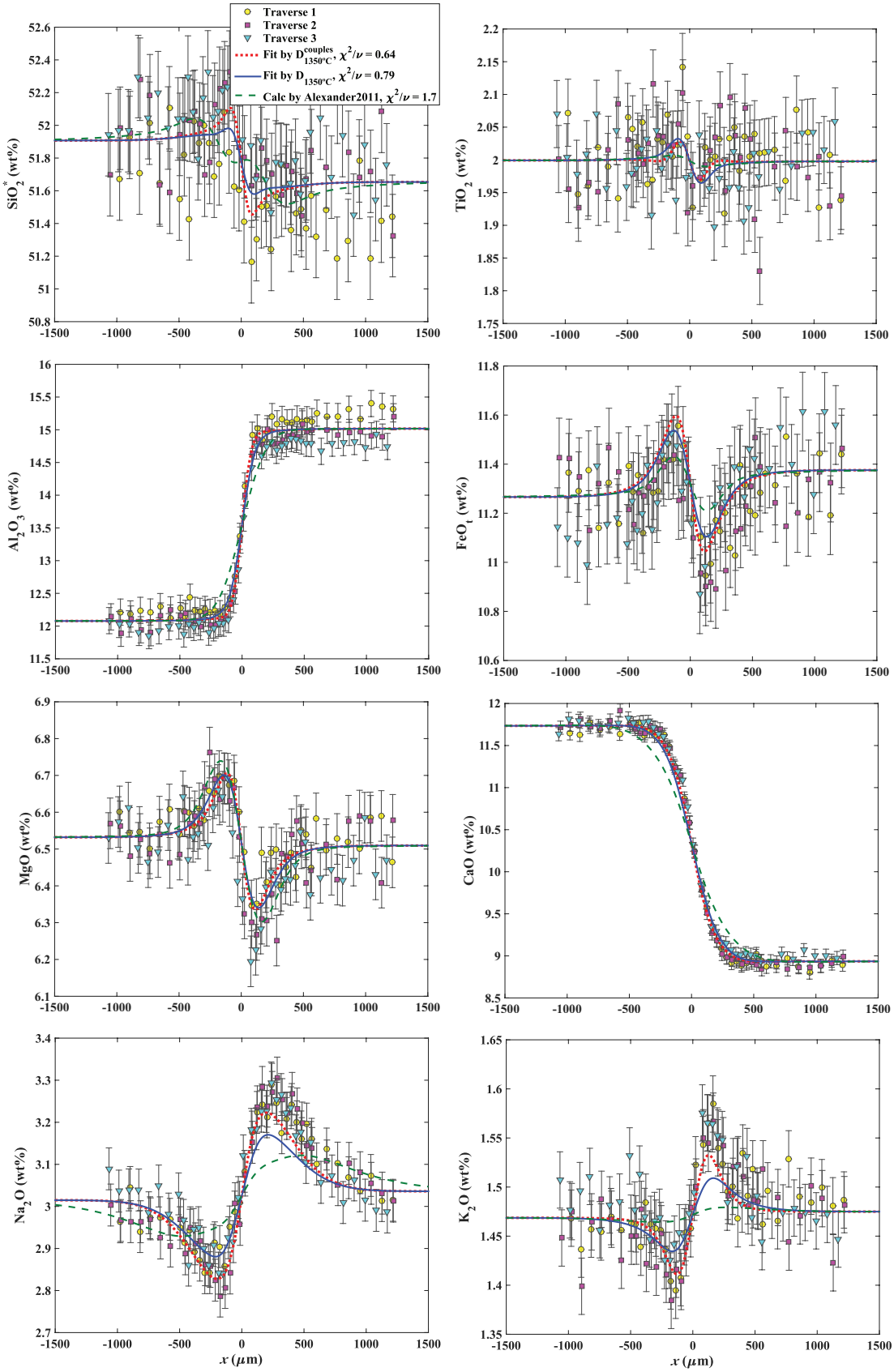

Fig. S10. Diffusion profiles of diffusion couple BS19&20A with predictions by diffusion matrix given by Alexander (2011) and fits by diffusion matrices $D^{couples}_{1350°C}$ in Table 4 and $D_{1350°C}$ in Table 5.

4. Predictions and fits for 9 diffusion couple and an anorthite dissolution experiments in iron-free haplobasaltic melts at 1500 ºC (Guo and Zhang, 2016)

Guo and Zhang (2016) reported a diffusion matrix in an iron-free 7-component haplobasaltic melt obtained from diffusion couple experiments at ~1500 ºC and at 1 GPa. They also carried out an anorthite dissolution experiment at ~1500 ºC and at 1 GPa in the same melt to examine the applicability of the obtained diffusion matrix. They showed that it is possible to predict diffusion profiles during anorthite dissolution using this diffusion matrix, but there is small discrepancy, especially for K_2O. Here, we fit both the diffusion couple and anorthite dissolution experiments to obtain a new diffusion matrix in this melt (Table 7). The fits for the diffusion profiles during anorthite dissolution are excellent (Fig. S20) with overall χ^2/ν = 1.2. The fits for the diffusion profiles in the diffusion couple experiments are also excellent and shown by solid curves in Figs. S11–S19 in the supplementary file. This new diffusion matrix is preferred over the diffusion matrix reported by Guo and Zhang (2016), and we recommend the use of the new diffusion matrix (Table 7) for this 7-component haplobasaltic melt.

In Figs. S11–S20, all the points represent the measured data, and the different styles of the symbols indicate different traverses. All the fits for all 9 diffusion couple experiments and predictions for an anorthite dissolution experiment by diffusion matrix given by Guo and Zhang (2016) are shown by short-dashed curves in Figs. S11–S20. All the fits for all 9 diffusion couple and an anorthite dissolution experiments by a new diffusion matrix in Table 7 are shown by solid curves in Figs. S11–S20.

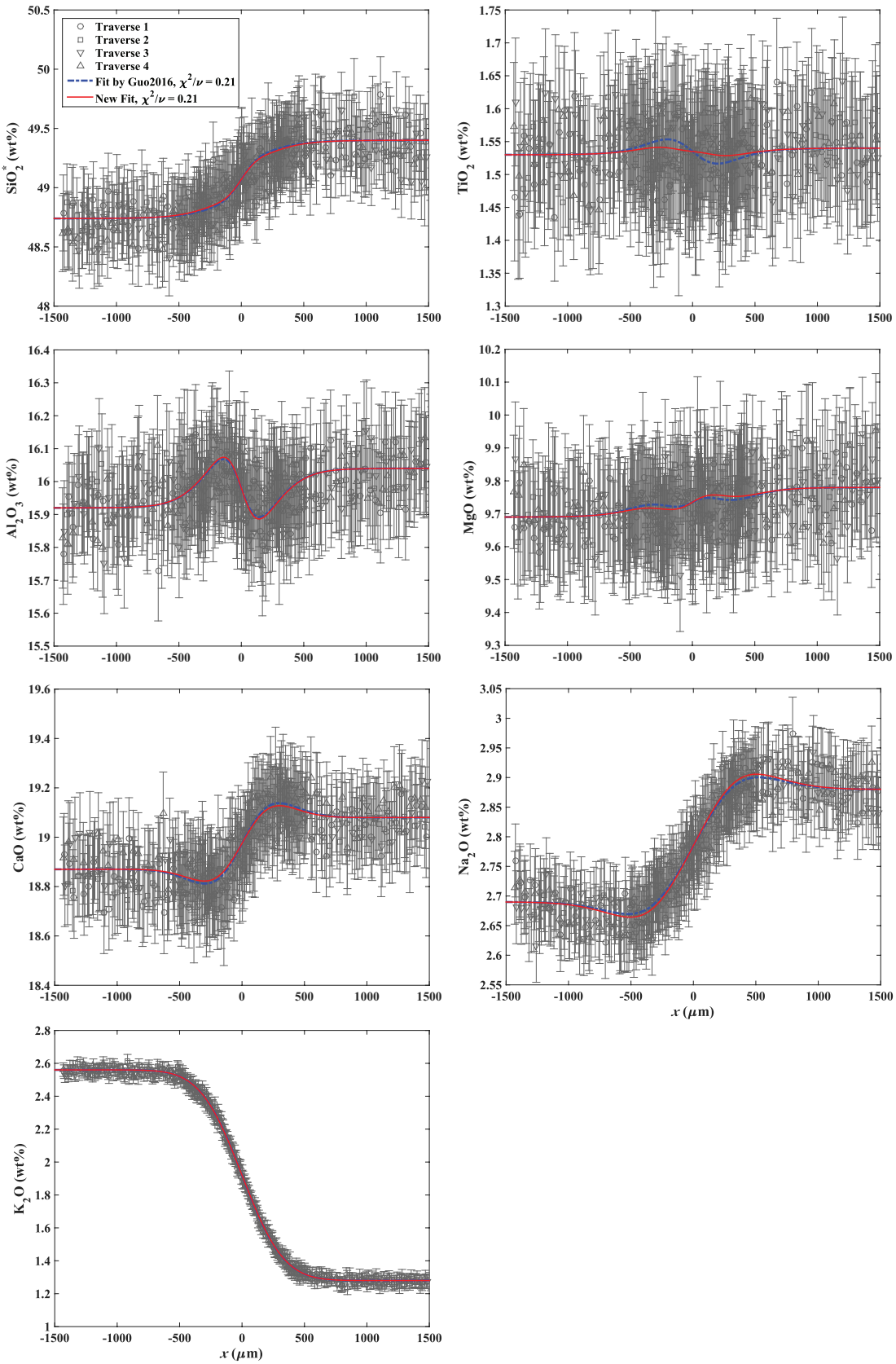

Fig. S11. Diffusion profiles of diffusion couple HB2&4A with fits by diffusion matrix given by Guo and Zhang (2016) and a new diffusion matrix in Table 7.

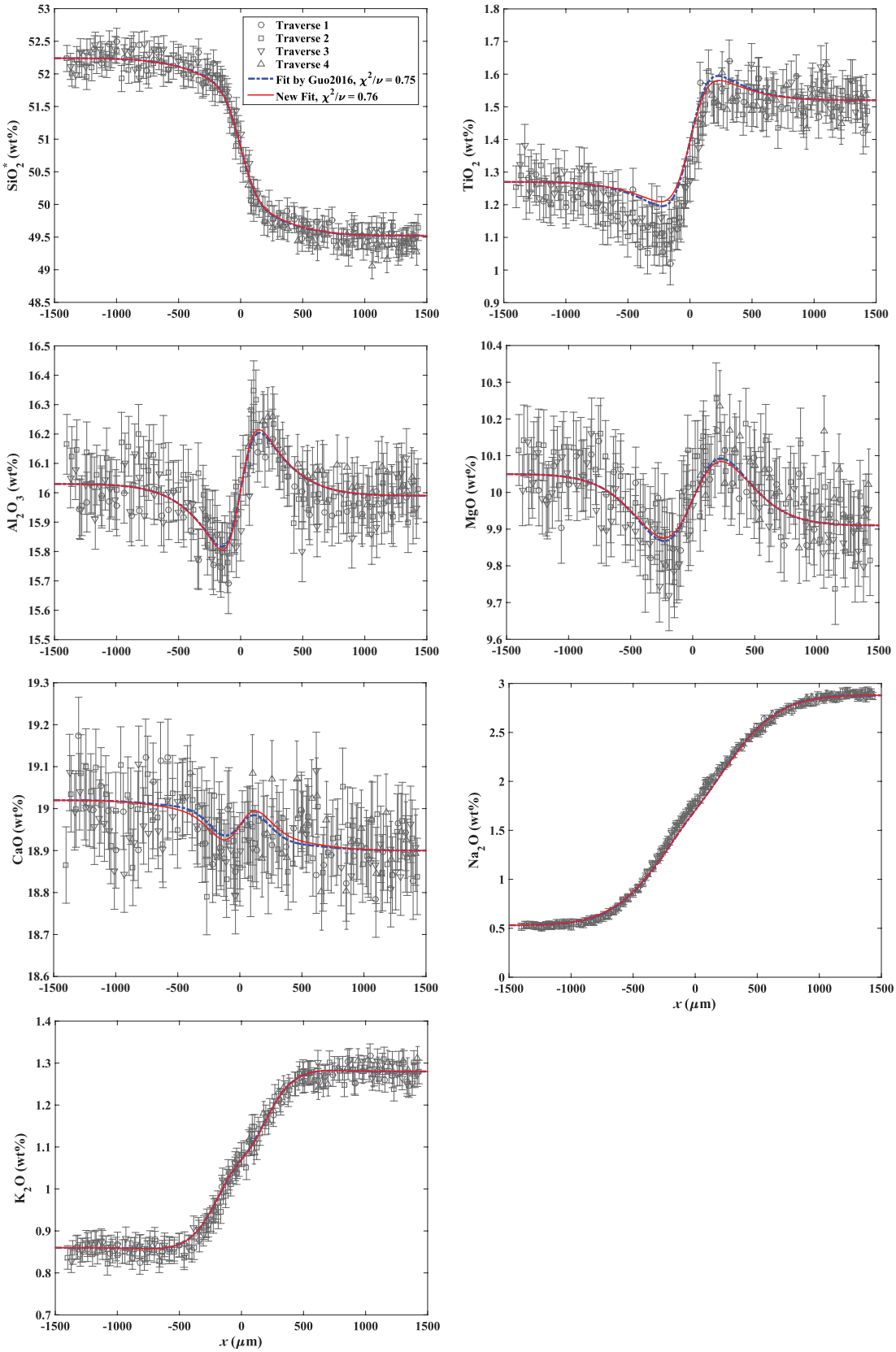

Fig. S12. Diffusion profiles of diffusion couple HB3&4A with fits by diffusion matrix given by Guo and Zhang (2016) and a new diffusion matrix in Table 7.

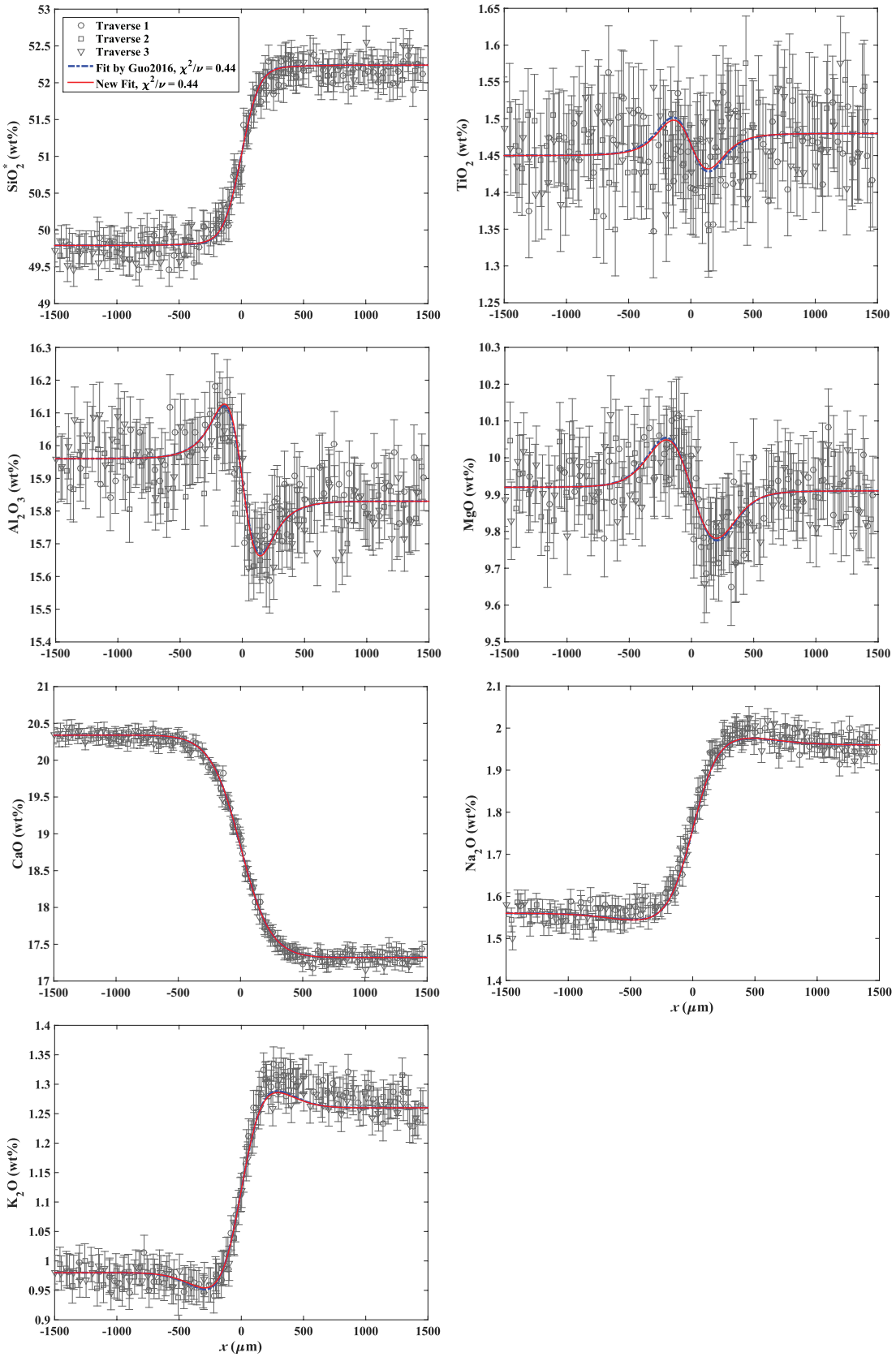

Fig. S13. Diffusion profiles of diffusion couple HB5&6A with fits by diffusion matrix given by Guo and Zhang (2016) and a new diffusion matrix in Table 7.

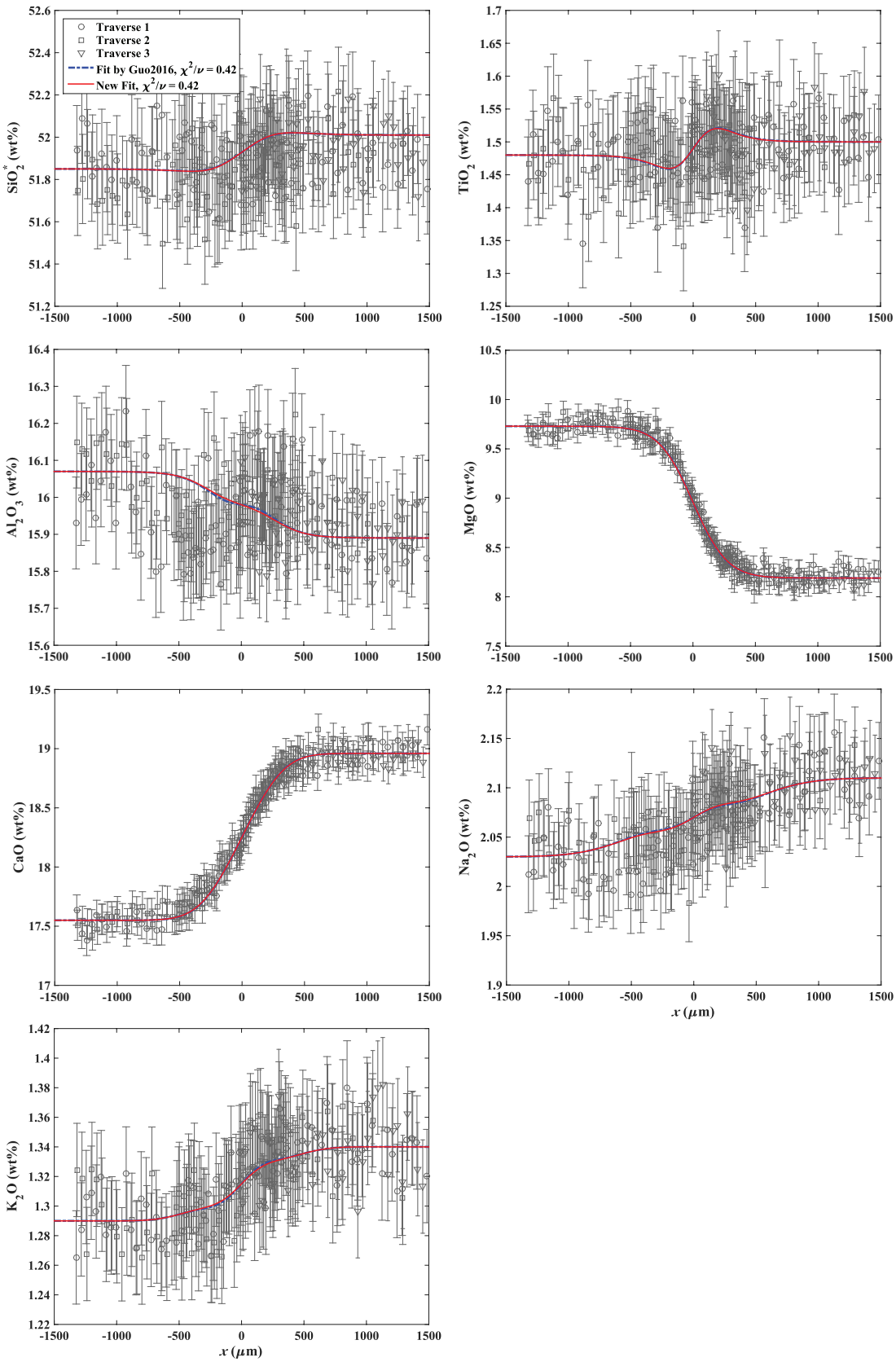

Fig. S14. Diffusion profiles of diffusion couple HB5&7A with fits by diffusion matrix given by Guo and Zhang (2016) and a new diffusion matrix in Table 7.

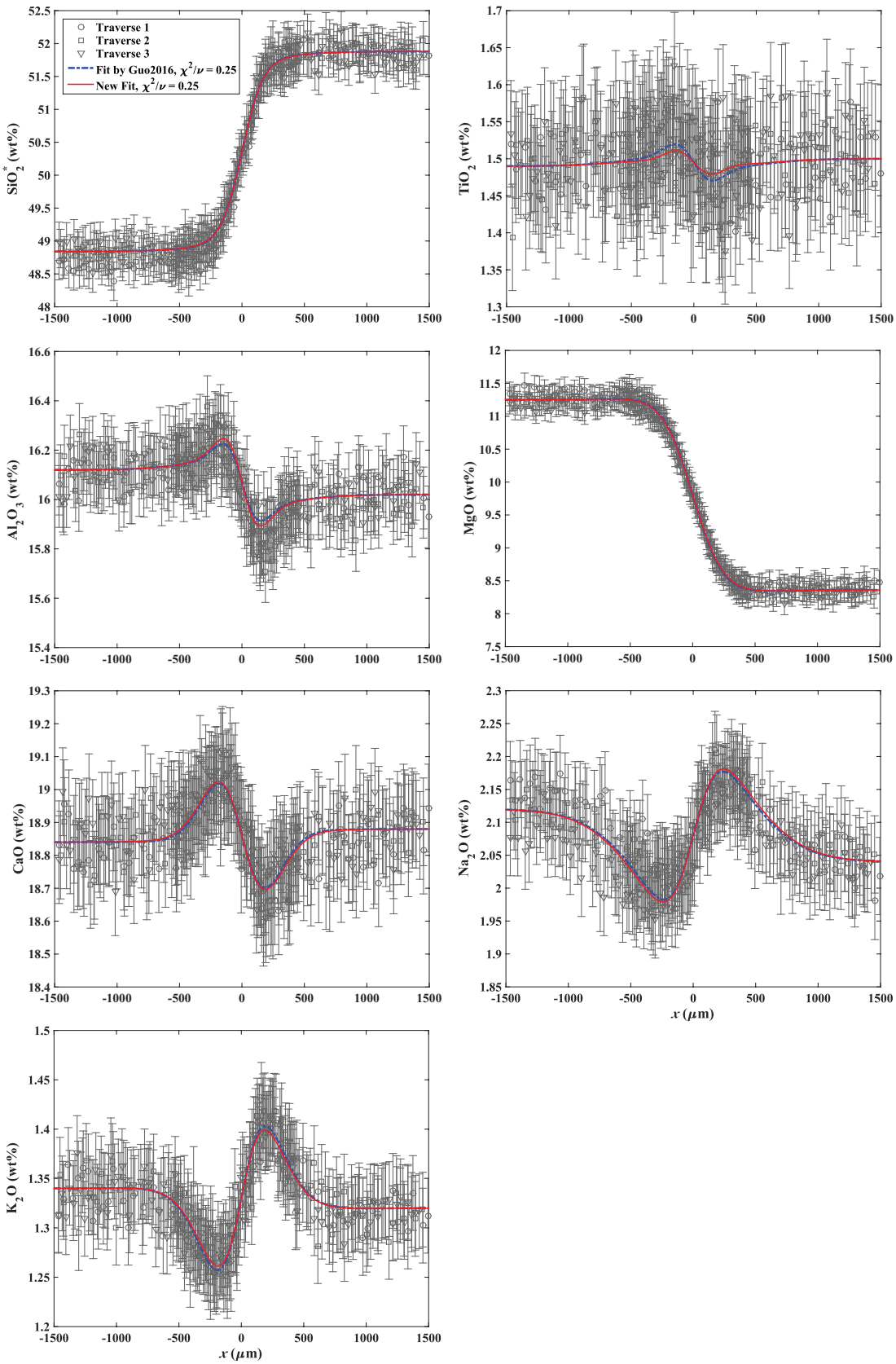

Fig. S15. Diffusion profiles of diffusion couple HB7&8B with fits by diffusion matrix given by Guo and Zhang (2016) and a new diffusion matrix in Table 7.

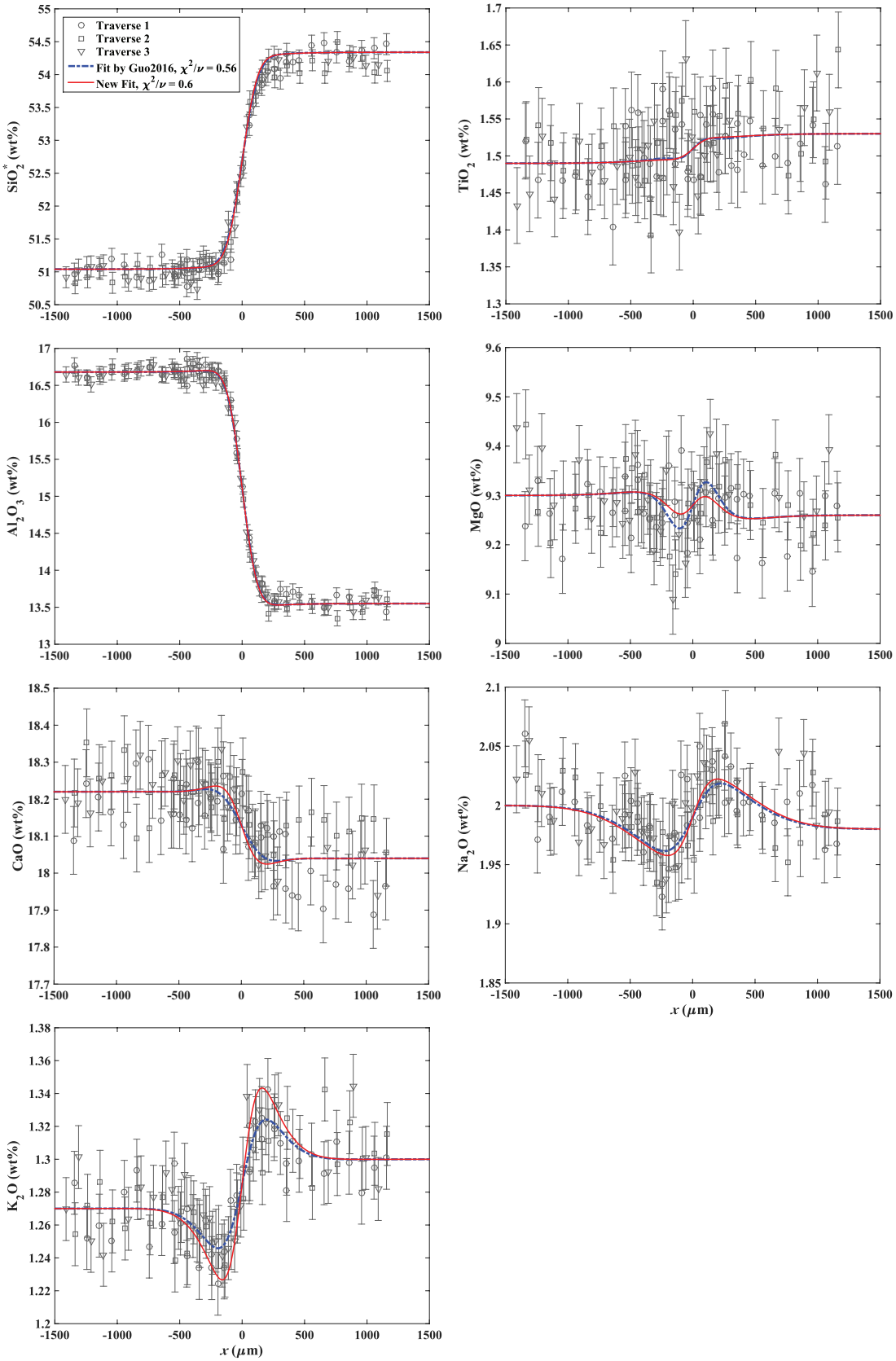

Fig. S16. Diffusion profiles of diffusion couple HB9&10A with fits by diffusion matrix given by Guo and Zhang (2016) and a new diffusion matrix in Table 7.

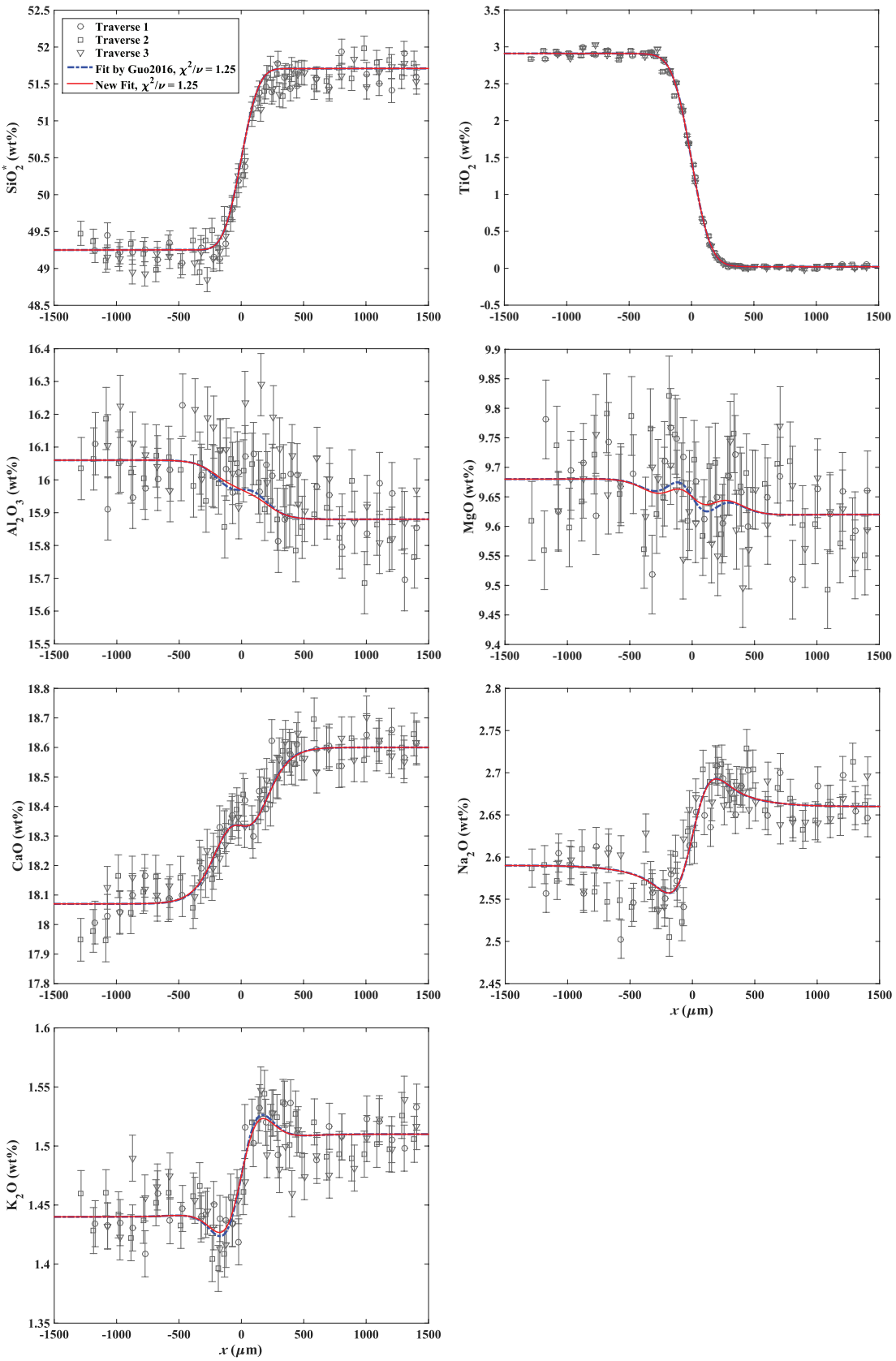

Fig. S17. Diffusion profiles of diffusion couple HB11&12F with fits by diffusion matrix given by Guo and Zhang (2016) and a new diffusion matrix in Table 7.

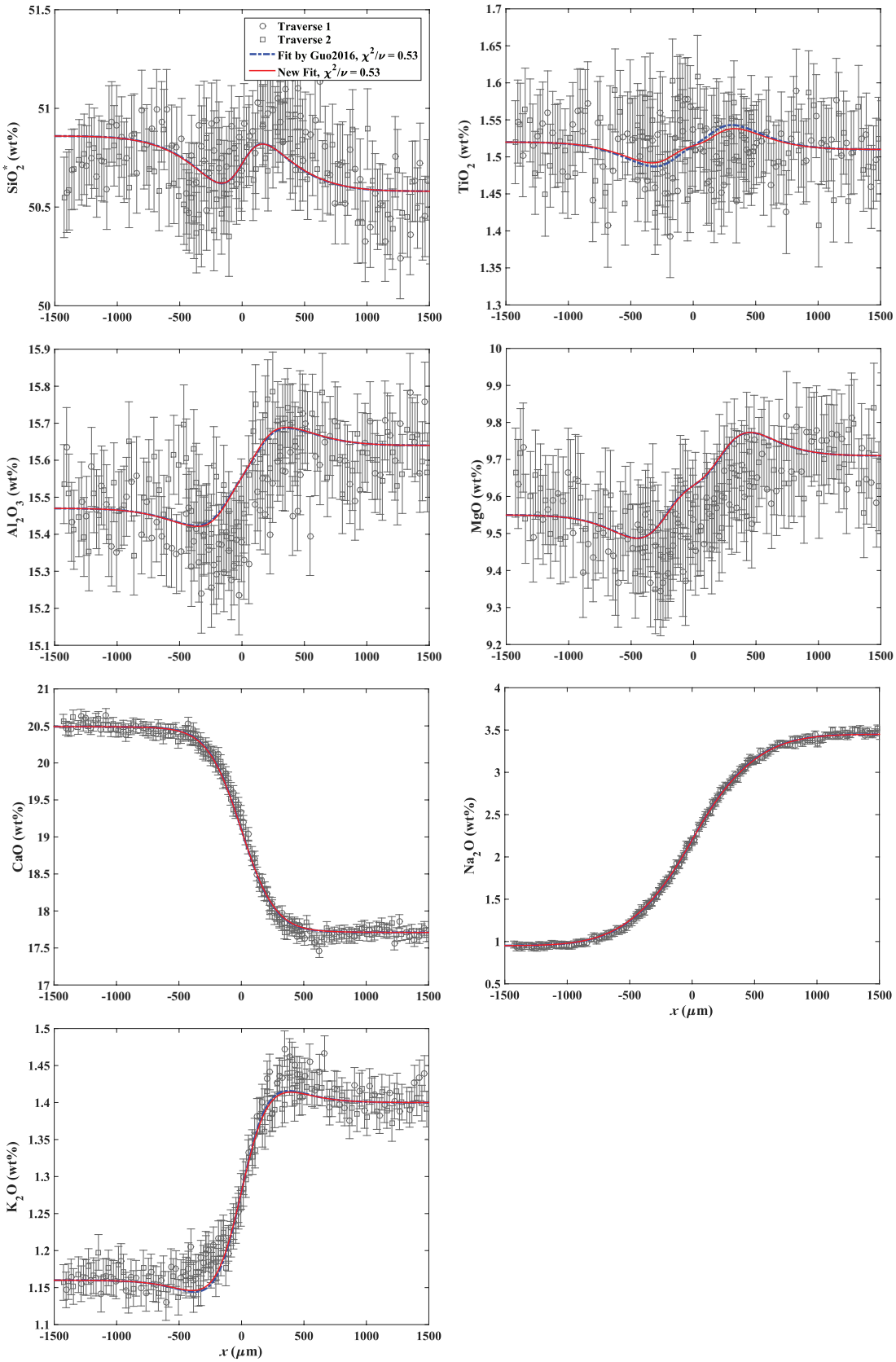

Fig. S18. Diffusion profiles of diffusion couple HB15&16A with fits by diffusion matrix given by Guo and Zhang (2016) and a new diffusion matrix in Table 7.

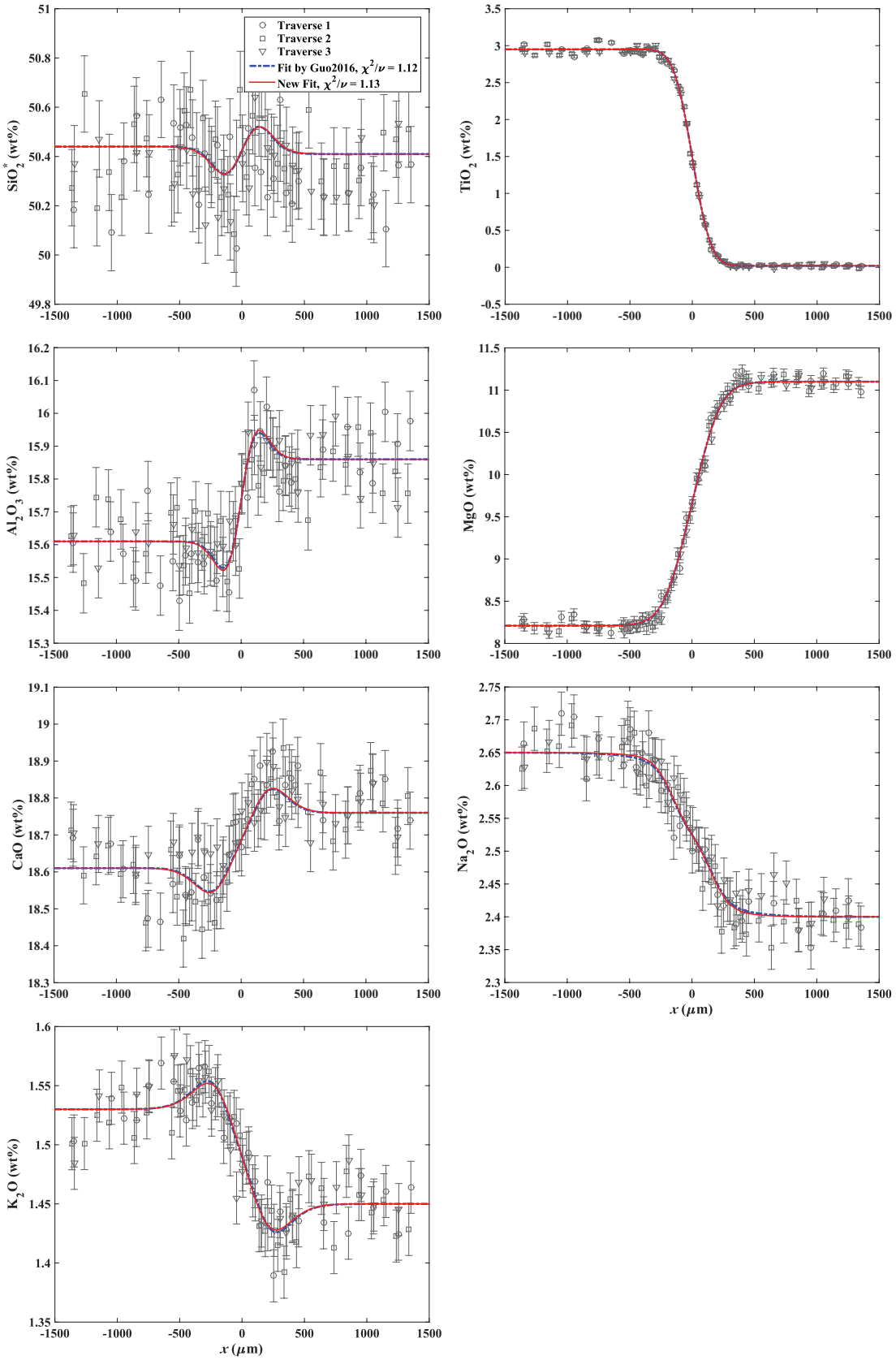

Fig. S19. Diffusion profiles of diffusion couple HB17&18A with fits by diffusion matrix given by Guo and Zhang (2016) and a new diffusion matrix in Table 7.

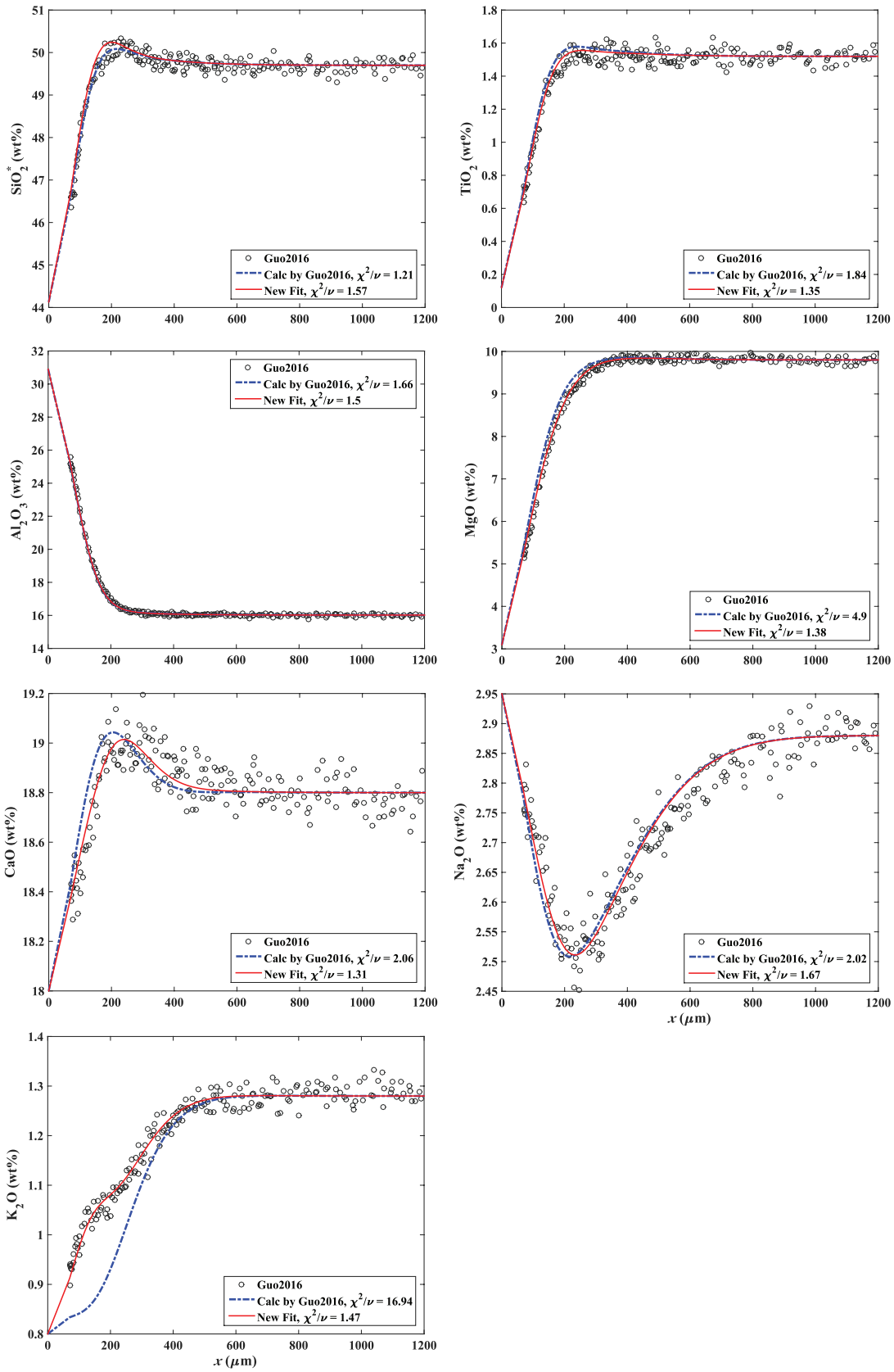

Fig. S20. Diffusion profiles of anorthite dissolution An&HB4 with predictions by diffusion matrix given by Guo and Zhang (2016), and fits by a new diffusion matrix in Table 7.